Phys. Chem. Chem. Phys., 2012, **14**, 3208–3218

# First principles study of sulfuric acid anion adsorption on Pt(111) electrode

**Ryosuke Jinnouchi,[a]* Tatsuya Hatanaka,[a] Yu Morimoto,[a] and Masatoshi Osawa[b]**

A first principles theory combined with a continuum electrolyte theory is applied to adsorption of sulfuric acid anions on Pt(111) in 0.1 M $H_2SO_4$ solution. The theoretical free energy diagram indicates that sulfuric acid anions adsorb as bisulfate in the potential range of $0.41 < U \leq 0.48$ V (RHE) and as sulfate in 0.48 V (RHE) < $U$. This diagram also indicates that sulfate inhibits formations of surface oxide and hydroxide. Charge analysis shows that the total charge transferred for the formation of the full coverage sulfate adlayer is 90 $\mu C \cdot cm^{-2}$, and that the electrosorption valency value is −0.45 to −0.95 in $0.41 < U \leq$ 0.48 V (RHE) and −1.75 to −1.85 in $U >$ 0.48 V (RHE) in good agreement with experiments reported in the literature. Vibration analysis indicates that the vibration frequencies observed experimentally at 1250 and 950 $cm^{-1}$ can be assigned, respectively, to the S-O (uncoordinated) and symmetric S-O stretching modes for sulfate, and that the higher frequency mode has a larger potential-dependence (58 $cm^{-1} \cdot V^{-1}$) than the lower one.

## 1. Introduction

Since the first invention of fuel cells by Sir Grove in 1839,[1] studies on interfaces between sulfuric acid solution and platinum have widely attracted attentions of electrochemists and surface scientists. In particular, the specific adsorption of sulfuric acid anion on platinum has been extensively studied. From state-of-the-art experiments on Pt(111), a wide range of valuable information has been obtained on various aspects of the interfacial phenomena including specific features observed in cyclic voltammetry (CV),[2–7] atomic structures,[8–10] electrosorption valency[4, 11] and vibration frequencies.[5, 12–21] However, there still remains an essential question: which is the major adsorbate, sulfate or bisulfate? Because of this unresolved question, one cannot exactly describe the charge distribution in the electric double layer and its formation reaction formula for this most conventional fuel cells electrode.

This question is exemplified by contradicting interpretations of absorption bands at 1250 and 950 $cm^{-1}$ measured by *in situ* infrared reflection absorption spectroscopy (IRAS) in sulfuric acid solutions, where bisulfate is the major anion. Faguy et al.,[12] Nichols,[13] and Ito and co-workers[14] interpreted the bands as the preferential adsorption of bisulfate, while Nart and co-workers interpreted the bands as the preferential adsorption of sulfate.[15] Later, Faguy et al. interpreted the bands as the preferential adsorption of hydronium-sulfate ion pair.[16] Lanchenwitzer and Lipkowski further studied on this system and interpreted the bands as the preferential adsorption of bisulfate at pH < 3.3 and sulfate at pH > 4.7.[18] Recently, Su et al. interpreted the bands as the preferential adsorption of sulfate at $1 \leq$ pH $\leq 5.6$.[21] Despite intensive experiments, a consensus has not been reached yet.

Recently, atomistic simulations using the density functional theory (DFT)[22, 23] has become applicable to investigate reactions at electrified liquid-solid interfaces.[24–29] These simulations have provided valuable information on several electrocatalytic reactions,[30–35] but a very few studies has been reported regarding the specific adsorption of the sulfuric acid anions on Pt(111). Santana et al. applied a cluster model approach to this issue first,[36] and concluded that the preferential adsorbate is bisulfate in $0.30 < U \leq 0.45$ V (RHE), hydronium-sulfate ion pair in $0.45 < U \leq 0.70$ V (RHE), and sulfate in 0.70 V (RHE) < $U$.

In this study, a theoretical method using DFT on an extended slab model, which correctly describe the metallic nature of the electrode, is applied to this issue. Theoretical methodologies are described in section 2. Results and discussion are presented from sections 3 to 5. Conclusions are summarized in section 6.

## 2. Computational method

Before describing the computational method, we briefly describe the system considered in this study and definitions of the reference state.

The system is a Pt(111) electrode in a 0.1 $mol \cdot L^{-1}$ $H_2SO_4$

[a] *Toyota Central Research & Development Laboratories, Inc., Nagakute, Aichi 480-1192, Japan. Fax: +81-561-71-4120; Tel: +81-561-61-7290; E-mail: e1262@mosk.tytlabs.co.jp*

[b] *Catalysis Research Center, Hokkaido University, Sapporo 001-0021, Japan. Fax: +81-11-706-9123; Tel: +81-11-706-9124; E-mail: osawam@cat.hokudai.ac.jp*

† Electronic Supplementary Information (ESI) available: [equations for a mean field by a solvation medium, equations for a continuum solvation theory, enthalpies and entropies of motions of atoms nuclei, preliminary results on vibration frequencies of several molecules, clusters and surface slabs in vacuum, and displacement vectors of vibration modes]. See DOI: 10.1039/b000000x/

solution at 298.15 K and 1 atm. From the standard Gibbs free energies,[37] concentrations of ions in the bulk solution are calculated as 0.11 mol·L$^{-1}$ for $H^+$(aq), 0.09 mol·L$^{-1}$ for $HSO_4^-$(aq) and 0.01 mol·L$^{-1}$ for $SO_4^{2-}$(aq). In this article, (g), (aq) and (ads) mean gas phase, aqueous phase and adsorbed phase, respectively.

The reference state is defined as 298.15 K for the temperature, 1 atm for pressures of $H_2$(g), $H_2O$(g), $HSO_4^-$(g) and $H^+$(g), and 1 mol·L$^{-1}$ for $H^+$(aq) and $HSO_4^-$(aq). For states other than the reference, the Gibbs free energy is calculated by the Nernst equation. For adsorbates, we neglected the activity term, e.g. $k_BT$ ln [ $\theta/(1-\theta)$], where $k_B$ is the Boltzmann constant, and $\theta$ is the surface coverage. By this term, the Gibbs free energy is decreased when the surface coverage decreases, but the decrease in the Gibbs free energy is small and does not change conclusions given in this study.

### 2.1 Basic equations

For reducing the computational cost needed to handle the solid-liquid interface under a long-ranged electric double layer by DFT, we divide the system into two regions: (i) the interfacial region comprising of adsorbed water molecules and ions and the surface, and (ii) the region far from the interface.[29, 33] In the region (i), chemical bonds in the adsorbates are accurately described by DFT. In contrast, the region (ii) is viewed as a static medium creating a mean field of the solvation surrounding the molecules, ions and surface in the region (i). It has been demonstrated that a continuum medium models well describe mean fields of the solvations,[29, 33, 38–45] and therefore, a modified Poisson-Boltzmann theory[46, 47] is applied to this region. The system is opened for electrons in the region (i) and ions in the region (ii). The electrochemical potential (Fermi energy) of the electrons is controlled by an external circuit, and chemical potentials of the ions are the same as those in the bulk electrolyte in contact with the system. Details of the (electro)chemical potentials are described later in this section and Supplementary Information.

Atoms in the region (i) are regarded as mass points moving on an effective potential energy surface $E_1$ comprising of a gas phase potential energy surface $E_0$ plus the mean field of the solvation $G_m$ as follows,

$$E_1[\{\mathbf{R}_\alpha\}] = E_0[\{\mathbf{R}_\alpha\}] + G_m[\{\mathbf{R}_\alpha\}], \quad (1)$$

where $\mathbf{R}_\alpha$ is the position vector of the $\alpha$th atomic nuclei in the region (i). As described in section A in the Supplementary Information or a textbook,[48] $G_m$ is a potential averaged over a phase space of all the atoms in the region (ii) at fixed $\{\mathbf{R}_\alpha\}$. The statistical average is executed at certain temperature, pressure and chemical potentials for electrons and ions. Hence, those parameters also affect $G_m$.

In actual computations in this study, $E_1$ is obtained by a self-consistent reaction field (SCRF) calculation on the DFT system combined with the modeled continuum electrolyte instead of the statistical average over the phase space of explicit molecules and ions. In this model, $E_1$ is described as follows,

$$E_1[\{\mathbf{R}_\alpha\}] = K + E_{xc} + E_{es} - T_eS_e + G_{ss,nes} + G_{is,nes} - TS_i + G_{mc}, \quad (2)$$

where $K$, $E_{xc}$ and $E_{es}$ are the kinetic, exchange-correlation, electrostatic energies, respectively, and $T_e$ and $S_e$ are the electronic temperature and entropy, respectively. $G_{ss,nes}$ is a free energy based on non-electrostatic interactions between atoms in the region (i) and water molecules in the region (ii). $G_{is,nes}$ is a free energy based on non-electrostatic interactions between atoms in the region (i) and ions in the region (ii). $S_i$ is the entropy of the electrolyte in the region (ii), and $T$ is the temperature. $G_{mc}$ is the mass conservation term, which takes account of a change in the Gibbs free energy caused by changes in the numbers of electrons in the region (i) and ions in the region (ii). Although details of those terms were described elsewhere,[29, 35] we briefly describe its physical background in section B in the Supplementary Information.

$E_1$ is also a functional of wave functions $\{\psi_n\}$ for electrons in region (i), occupation numbers $\{f_n\}$ of the wave functions, ion densities $\rho_\pm$ in the region (ii) and the electrostatic potential $\phi$ in the whole system. These variables are determined to minimize $E_1$ by solving simultaneous equations obtained by variational principles as follows,

$$\left[-\frac{1}{2}\nabla^2 + \frac{\delta E_{xc}}{\delta \rho_e} + \phi(\mathbf{r})\right]\psi_n(\mathbf{r}) = \varepsilon_n \psi_n(\mathbf{r}), \quad (3)$$

$$\nabla\cdot(\varepsilon(\mathbf{r})\nabla\phi(\mathbf{r})) = -4\pi(\rho_e(\mathbf{r}) + \rho_c(\mathbf{r}) + \rho_-(\mathbf{r}) + \rho_+(\mathbf{r})), \quad (4)$$

$$\rho_\pm(\mathbf{r}) = \mp\frac{c_b e^{(\pm\phi(\mathbf{r})-\phi_{rep}(\mathbf{r}))/k_BT}}{1-2a^3c_b+2a^3c_b\cosh(\phi(\mathbf{r})/k_BT)e^{-\phi_{rep}(\mathbf{r})/k_BT}}, \quad (5)$$

$$\rho_e(\mathbf{r}) = \sum_n f_n|\psi_n(\mathbf{r})|^2, \quad (6)$$

$$T_e\frac{\partial S_e}{\partial f_n} = \varepsilon_n - \varepsilon_F, \quad (7)$$

$$\int \psi_n^*(\mathbf{r})\psi_m(\mathbf{r})d\mathbf{r} = \delta_{nm}, \quad (8)$$

$$\sum_n f_n = N, \quad (9)$$

where $\rho_e$ is the electron density, $\varepsilon_n$ is the eigenenergy of the $n$th electronic state, $\phi_{rep}$ is the non-electrostatic repulsive potential between atoms in the region (i) and ions in the region (ii), $\varepsilon_F$ is the Fermi energy, $N$ is the number of the electrons, and $c_b$ and $a$ are the ion concentration in the bulk electrolyte and the radius of ion, respectively, which are 0.1 mol·L$^{-1}$ and 3 Å in this study. There is an arbitrariness in the choice of $a$, but results are insensitive to the parameter. Eqn (5) is derived from a modified Poisson-Boltzmann theory for a symmetric 1:1 electrolyte, which describes well the actual composition of 0.1 mol·L$^{-1}$ $H_2SO_4$ solution. Details of the physical background of the parameters in eqn (5) are described in the section B in the Supplementary Information or a previous publication.[29]

The Gibbs free energy at the reference state is obtained by a statistical average over a phase space of atoms in the region (i). The integration uses simple statistical models for molecules and adsorbates (see details in the section C in the Supplementary Information). For molecules and ions in a homogeneous gas phase or aqueous phase, translation, rotation, and vibration motions are included. For adsorbates, only vibration motions are taken into account. The Gibbs free energy is described as follows,

$$G = E_1\left[\left\{\mathbf{R}_\alpha^{\,0}\right\}\right] + H_n - TS_n\,, \tag{10}$$

where $\mathbf{R}_\alpha^{\,0}$ is the $\alpha$th equilibrium atomic position vector, $H_n$ and $S_n$ are the respective enthalpy and entropy of the motions of the atoms. The equilibrium positions $\{\mathbf{R}_\alpha^{\,0}\}$ are determined to minimize $E_1$. All the values of $H_n$ and $S_n$ are tabulated in Table S1 in the Supplementary Information.

The electrochemical potential (Fermi energy) $\varepsilon_F$ of the electrons at the equilibrium atomic positions $\{\mathbf{R}_\alpha^{\,0}\}$ are converted to the electrode potential $U$ in the standard hydrogen electrode (SHE) scale by using the Fermi energy $\phi_{\mathrm{SHE}}$ of the SHE as follows,

$$U = -\frac{\varepsilon_F - \phi_{\mathrm{SHE}}}{e}\,, \tag{11}$$

where $e$ is the elementary charge. $\phi_{\mathrm{SHE}}$ is obtained as –4.555 eV by using theoretical Gibbs free energies of $H_2$(g) and $H^+$(aq), which will be described in section 2.5. The electrode potential scaled with a reversible hydrogen electrode (RHE) is obtained by using the Nernst equation as follows,

$$U = -\frac{\varepsilon_F - \phi_{\mathrm{SHE}}}{e} + \frac{k_B T \ln 10}{e}\mathrm{pH}\,. \tag{12}$$

### 2.2 Reaction free energies and numbers of transferred electrons

Here, we consider electrode reactions forming a surface state $i$, $j$ or $k$ from a reference surface state R. For the given surface state, the free energy $G_l$ ($l$ = R, $i$, $j$ or $k$) defined as eqn (10) is obtained by solving eqn (3) to (9) changing the total number of electrons $N_l$. The electrode potential $U_l$ corresponding to the given $N_l$ is also obtained from the electrochemical potential of electrons (Fermi energies) $\varepsilon_{F,l}$. Then, $G_l$ and $N_l$ are plotted as functions of the electrode potential $U$ as shown in Figs. 1 (A) and (B), and these functions are approximated by quadratic functions as follows,

$$G_l(U) \cong a_l U^2 + b_l U + c_l\,, \tag{13}$$

$$N_l(U) \cong s_l U^2 + t_l U + u_l\,. \tag{14}$$

Finally, the reaction free energies and the number of transferred electrons are obtained as functions of $U$ as follows,

$$\Delta G_l(U) \cong (a_l - a_\mathrm{R})U^2 + (b_l - b_\mathrm{R})U + (c_l - c_\mathrm{R})\,, \tag{15}$$

$$\Delta N_l(U) \cong (s_l - s_\mathrm{R})U^2 + (t_l - t_\mathrm{R})U + (u_l - u_\mathrm{R})\,. \tag{16}$$

### 2.3 Vibration frequencies

Vibration frequencies are obtained as eigenvalues of Hessian matrices, which are the second derivatives of the effective potential energy surface $E_1$ with respect to positions of nuclei $\{\mathbf{R}_\alpha\}$. Similarly to the Gibbs free energy in eqn (10), $E_1$ also depends on the electrode potential $U$; therefore, the vibration frequencies also depend on $U$.

Strictly speaking, atoms vibrate under not the averaged potential energy surface $E_1$ but a potential energy surface determined from an instantaneous atomic configuration. Hence, some errors will be made by using the methodology described above. It is, however, expected that the methodology reasonably includes the field effects of the long-ranged electric double layer, because the time scale of the formation of the electric double layer is much longer than that of the vibrations, and therefore, its field can be approximated well by the averaged potential. The same idea have been used in computations on molecules and ions in homogeneous solutions.[49, 50] Similar ideas have been also successfully utilized to investigate Stark effects on vibrations of CO(ads) and H(ads) where the mean field $G_m$ was described by a simple constant electric field.[51–53]

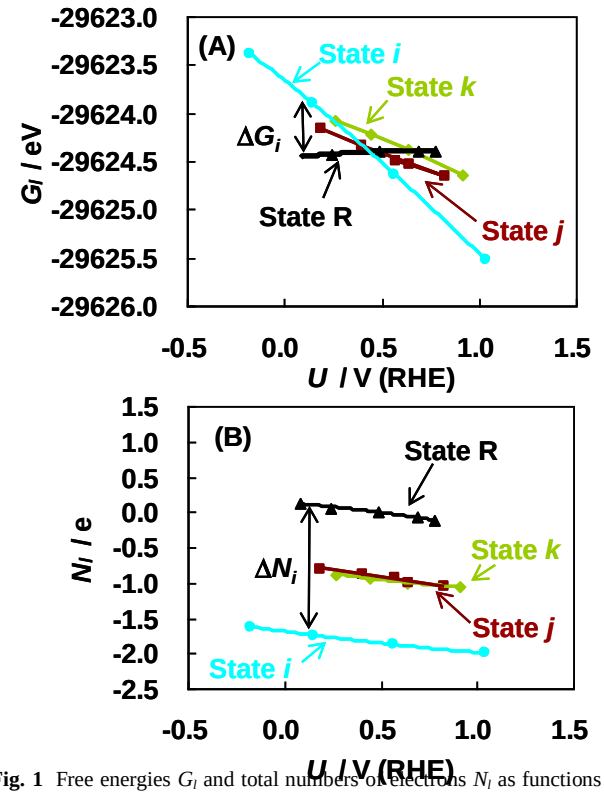


**Fig. 1** Free energies $G_l$ and total numbers of electrons $N_l$ as functions of the electrode potential $U$. The subscript $l$ indicates a surface state R, $i$, $j$ or $k$. The data shown in this figure are the first principle results for R: $H_2O$(ads) (black), $i$: sulfate (light blue), $j$: bisulfate (light green) and $k$: mixture of bisulfate and hydronium-sulfate ion pair (brown).

### 2.4 Adsorption reactions

The reference state $l$ = R is defined as the surface covered by adsorbed water ($H_2O$(ads)), and the surface state $l = i, j, k\cdots$ are defined as the surface covered by either sulfate ($SO_4$(ads)), bisulfate ($HSO_4$(ads)), hydronium-sulfate ion pair ($H_3O$-$SO_4$(ads)), hydrogen (H(ads)), hydroxyl (OH(ads)) or oxygen (O(ads)).

Accordingly, the reactions forming the state $l = i, j, k\cdots$ from the reference state $l$ = R can be described as follows,

$$\mathrm{HSO_4^-(aq)} + * \rightarrow \mathrm{SO_4^{\delta_1}(ads)} + \mathrm{H^+(aq)} + (2+\delta_1)\mathrm{e^-}\,, \tag{17}$$

$$\mathrm{HSO_4^-(aq)} + * \rightarrow \mathrm{HSO_4^{\delta_2}(ads)} + (1+\delta_2)\mathrm{e^-}\,, \tag{18}$$

$$HSO_4^-(aq) + * \rightarrow H_3O\text{-}SO_4^{\delta_3}(ads) + (1+\delta_3)e^-, \quad (19)$$

$$H^+(aq) + * + (1-\delta_4)e^- \rightarrow H^{\delta_4}(ads), \quad (20)$$

$$H_2O(aq) + * \rightarrow OH^{\delta_5}(ads) + H^+(aq) + (1+\delta_5)e^-, \quad (21)$$

$$H_2O(aq) + * \rightarrow O^{\delta_6}(ads) + 2H^+(aq) + (2+\delta_6)e^-, \quad (22)$$

where * denotes an unoccupied surface site, and $\delta_i$ ($i$ = 1 to 6) are average charges of adsorbed species.

### 2.5 Atomistic models

**Models of molecules and ions** The first principles liquid water is assumed to have the same vapor pressure as real water: that is, $H_2O$(aq) is modeled as single water molecule with a vapor pressure $p_{H_2O(g)}$ of 0.035 atm at 298.15 K[54] as shown in Fig. 2 (A), and its Gibbs free energy is calculated as follows,

$$G[H_2O(aq)] = G[H_2O(g)] + k_B T \ln \frac{p_{H_2O(g)}}{p^0_{H_2O(g)}}, \quad (23)$$

where $p_{H2O(g)}{}^0$ = 1 atm.

The Gibbs free energy for $H^+$(aq) is calculated as follows,

$$G[H^+(aq)] = G[H^+(g)] + G_{solv}[H^+(aq)] + k_B T \ln c_{H^+(aq)} V_{gas}, \quad (24)$$

where $G_{solv}$ is the solvation free energy, $c_{H^+(aq)}$ is the concentration of $H^+$(aq), and $V_{gas}$ is the molar volume ( = 24.46 L·mol$^{-1}$) of the ideal gas at the reference state. $G_{solv}$ was calculated as the reaction free energy for the solvation reaction forming $H^+$ hydrated with four $H_2O$ molecules in the modeled continuum electrolyte (Fig. 2 (B)) from $H^+$ in the gas phase and four $H_2O$ molecules in the modeled continuum electrolyte (Fig. 2 (C)); this reaction is described as follows,

$$H^+(g) + (H_2O)_4(aq) \rightarrow H^+(H_2O)_4(aq). \quad (25)$$

This methodology is the same as those used in past theoretical studies.[29, 33, 55] Our result on $G_{solv}$ is −11.305 eV, which agrees with the past experimental and theoretical values of −11.379[56] and −11.372 eV,[55] respectively. The theoretical solvation free energy results in $\phi_{SHE}$ = −4.555 eV.

In a similar manner, the Gibbs free energy for $HSO_4^-$(aq) is calculated as follows,

$$G[HSO_4^-(aq)] = G[HSO_4^-(g)] + G_{solv}[HSO_4^-(aq)] + k_B T \ln c_{HSO^-(aq)} V_{gas}, \quad (26)$$

where $c_{HSO_4^-(aq)}$ is the concentration of $HSO_4^-$(aq). $G_{solv}$ for $HSO_4^-$(aq) is calculated as the reaction free energy for the solvation reaction forming $HSO_4^-$(aq) hydrated with four $H_2O$ molecules in the modeled continuum electrolyte (Fig. 2 (D)) from $HSO_4^-$(aq) in the gas phase and four $H_2O$ molecules in the modeled continuum electrolyte (Fig. 2 (C)); this reaction is described as follows,

$$HSO_4^-(g) + (H_2O)_4(aq) \rightarrow HSO_4^-(H_2O)_4(aq). \quad (27)$$

Our result on $G_{solv}$ is −2.256 eV, and this is within the range of the experimental error (−1.86±0.47 eV).[57]

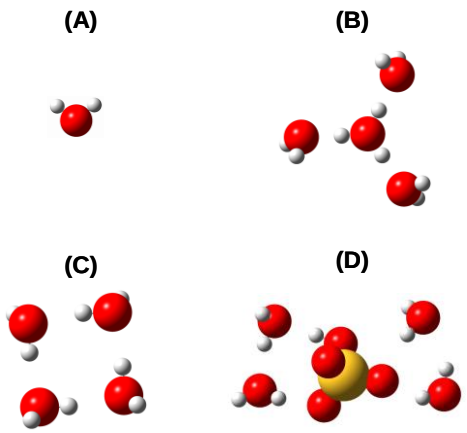


**Fig. 2** Models of (A) $H_2O$ in the gas phase, (B) $H^+$ hydrated with four $H_2O$ molecules in the modeled continuum electrolyte, (C) four $H_2O$ molecules in the modeled continuum electrolyte and (D) $HSO_4^-$ hydrated with four $H_2O$ molecules in the modeled continuum electrolyte. The yellow spheres are S, the small white spheres are H, and the red spheres are O.

**Models of surfaces** The surfaces with the adsorbed anions were modeled by 4 layer slabs with a 5×2√3 periodic structure shown in Figs. 3 (A), (B) and (C). At the full surface coverage of the anions, this periodic structure corresponds to the √3×√7 periodic structure observed in experiments.[8–10] Water molecules with an enlonged honeycomb structure proposed by Wan et al.[9] were placed on the slabs. Calculations were carried out for three anion coverages of $\theta_S$ = 0, 1/10 and 1/5 ML. The surface with $\theta_S$ = 0 ML was used as the reference state $l$ = R (the surface in the left hand state in the reactions (17)-(19)), and the surface with $\theta_S \neq 0$ ML was used as the state $l$ = $i$, $j$, $k$··· (the surface in the right hand state in the reactions (17)-(19)).

Surfaces with H(ads) and OH(ads) were modeled by 4 layer slabs with a 3×2√3 periodic structure shown in Figs. 4 (A) and (B), respectively, and surfaces with O(ads) were modeled by 4 layer slabs with a 3×2√3 and 6×2√3 periodic structures shown in Figs. 4 (C) and (D), respectively. On top of H(ads) and O(ads), water bilayers with a honeycomb structure[58, 59] were placed as shown in Figs. 4 (A), (C) and (D). In the case of OH(ads), a half dissociated water adlayer including OH(ads) and $H_2O$(ads) with a honeycomb structure [60–63] was placed on the slab as shown in Fig. 4 (B). Calculations on H(ads) and OH(ads) were carried out for two coverages of $\theta_H = \theta_{OH}$ = 0 and 1/3 ML, and calculations on O(ads) were carried out for three coverages of $\theta_O$ = 0, 1/3 and 1/2 ML. Similarly to the slabs with the adsorbed anions, the surface with $\theta_H = \theta_{OH} = \theta_O$ = 0 ML was used as the reference state $l$ = R (the surface in the left hand state in the reactions (20)-(22)), and the surface with $\theta_H = \theta_{OH} = \theta_O \neq 0$ ML was used as the state $l$ = $i$, $j$, $k$··· (the surface in the right hand state in the reactions (20)-(22)).

### 2.6 First principles calculations

**Calculations on solvated slab models** Calculations on the slabs in the modeled continuum electrolyte were carried out by a first principles code using linear combinations of pseudoatomic orbitals (LCPAOs) as basis sets and norm-conserving pseudopotentials as effective core potentials acting on valence electrons.[29, 33] A double zeta plus polarization (DZP) basis set with a cutoff radius of 3.5 Å was used for hydrogen, a double zeta plus double polarization (DZDP) basis set with a cutoff radius of 4.8 Å was used for oxygen, a DZDP

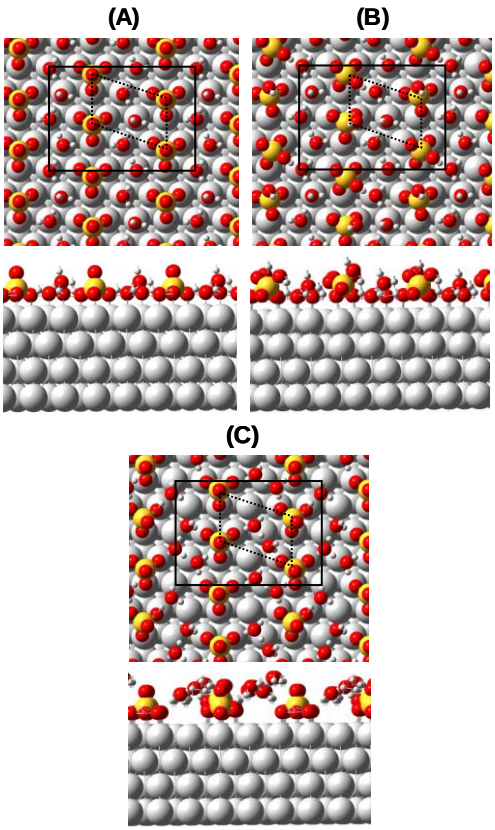


**Fig. 3** Top and side views of models for (A) $SO_4$(ads), (B) $HSO_4$(ads) and (C) $H_3O$-$SO_4$(ads). The squares with the solid lines in the top views are the unit cell with the $5\times2\sqrt{3}$ structure, and the parallelograms with the dashed lines show the $\sqrt{3}\times\sqrt{7}$ structure. The large white spheres are Pt, and other spheres are same as those in Fig. 2.

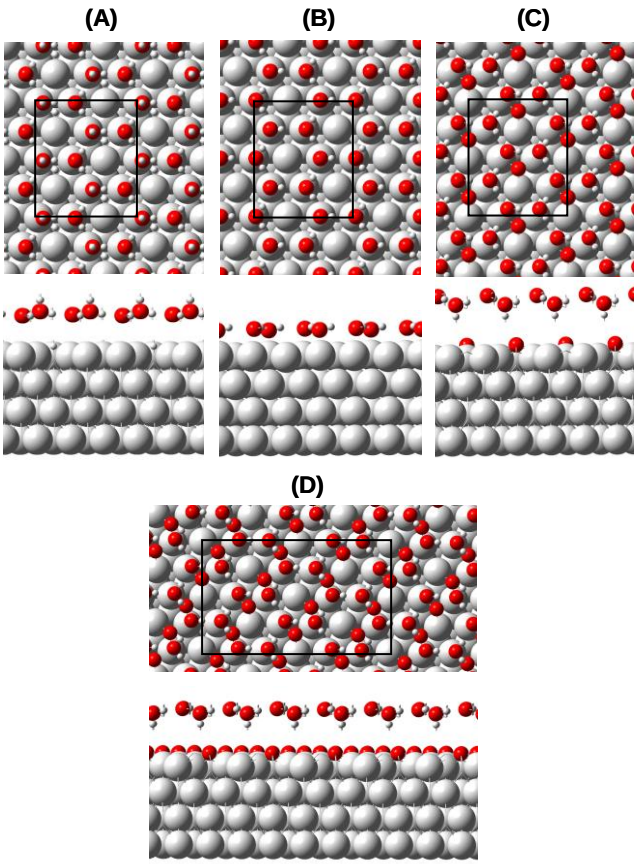


**Fig. 4** Top and side views of models for (A) H(ads), (B) OH(ads), (C) O(ads) (1/3 ML) and (D) O(ads) (1/2 ML). Squares in the top views are unit cells.

with an f-orbital (DZDP+f) basis set with a cutoff radius of 4.7 Å was used for sulfur, and a double zeta plus polarization (DZP) basis set with a cutoff radius of 4.9 Å was used for platinum.

Semi-local exchange-correlation functional of GGA-RPBE[64] that usually gives accurate adsorption energies was used to calculate the reaction free energies. On the other hand, GGA-PBE[65] was used to calculate vibrational frequencies because it gives better results as will be shown later.

Two dimensional periodic boundary conditions were applied for the slabs. Monkhorst-Pack **k**-point meshes of 3×3, 2×3 and 2×3[66] with a Gaussian smearing with an energy width of 0.1 eV[67] were used for $3\times2\sqrt{3}$, $5\times2\sqrt{3}$ and $6\times2\sqrt{3}$ unit cells, respectively. The periodic boundary conditions were not applied to the molecules and ions.

Parameters of $\beta = 1.3$ and $\rho_0 = 5.7\times10^{-4}$ a.u. for the modeled continuum electrolyte were used; definitions of these parameters are described elsewhere.[29] The grid spacing of 0.15 $Å^{-1}$ was used to solve the modified Poisson-Boltzmann equation by a fourth-order compact finite difference method.[68, 69]

Vibration frequencies were calculated as eigenvalues of Hessian matrices obtained through a finite difference method with an increment of 0.005 Å for the atomic positions. In this calculation, the Hessian matrices were approximated by the partial Hessian matrices of the adsorbates after checking the accuracy of this approximation by using the full Hessian matrices.

**Calculations on clusters by Gaussian03** To verify the accuracy of the GGA functionals, we also carried out calculations on vibration frequencies for molecules, ions and adsorbates modeled as clusters by Gaussian03.[70] Three theories, DFT using the semi-local GGA-PBE functional,[65] DFT using the non-local B3LYP functional[71] and the second order Møller-Plesset (MP2) theory,[72] were compared. The 6-311++G(2df,2pd)[73] basis sets were used for hydrogen, oxygen and sulfur, and the LANL2DZ basis set and effective core potential[74] were used for platinum. To examine the effect of the size of basis sets, other basis sets (aug-cc-pVDZ, aug-cc-pVTZ and aug-cc-pVQZ)[75–77] also were used for a $D_2SO_4$ molecule in vacuum.

## 3 Results and discussion: atomic structure, energy and electrosorption valency

### 3.1 Atomic structure

Optimized structures for three possible sulfuric acid anions, bisulfate, sulfate, and hydronium-sulfate ion pair, are shown in Fig. 5.

Two structures with a very small energy difference (0.01 eV) were found for bisulfate (A and B), in which bisulfate binds to the surface via two oxygen atoms. In structure A, a hydrogen bond is formed between bisulfate and adsorbed water, while in structure B, the hydrogen atom has an interaction with the dielectric medium. It should be also mentioned that the three O-Pt

bond lengths in structure B are longer than those in the previous theoretical result of 2.55, 2.57 and 3.35 Å at 0.40 V (RHE).[36] We further investigated the potential-dependence of the bond lengths and found that when the potential are increased from 0.32 to 0.97 V (RHE), the bond lengths are shortened from 2.61, 3.31 and 3.98 Å to 2.43, 3.18 and 3.81 Å, respectively, but are always longer than the previous results. This difference is mainly caused by the difference in the surface model between ours and the previous one; our model is the $5\times2\sqrt{3}$ periodic structure with a 1/5 ML surface coverage of bisulfate, and previous one is a cluster model with a much smaller surface coverage of 1/27 ML.

Sulfate is adsorbed at an *fcc* hollow site via three oxygen atoms with an approximately $C_{3v}$ symmetry (C), and its O-Pt bond lengths are shortened from 2.25, 2.27 and 2.34 Å to 2.20, 2.22 and 2.28 Å when the potential was increased from −0.11 to 1.10 V (RHE). Comparing with the result of bisulfate, the potential dependence is smaller. This is because sulfate is more rigidly bounded to the surface.

In hydronium-sulfate ion pair (D), sulfate is adsorbed at an *fcc* hollow site via three oxygen atoms as well and a pair of hydronium ion and a water molecule, more closer to Zundel ion ($H_5O_2^+$), is hydrogen bonded to uncoordinated oxygen atom of sulfate. At full sulfate coverage of $\theta_S$ = 1/5, one-fourths of the ion pairs were found to be changed to bisulfate. The O-Pt bond lengths are shortened from 2.22, 2.33 and 2.35 Å to 2.22, 2.28 and 2.29 Å when the potential was increased from 0.25 to 0.89 V (RHE), and its potential-dependence is slightly larger than that of sulfate.

### 3.2 Free energy diagram

Figure 6 shows the changes in Gibbs free energies $\Delta G_I$ per surface Pt atom as functions of the electrode potential $U$. In the absence of sulfuric acid anions, the most stable adsorbates are H(ads), $H_2O$(ads), OH(ads) and O(ads) in $U \le 0.11$ V, $0.11 < U \le 0.81$ V, $0.81 < U \le 1.00$ V and $1.00 \text{ V} < U$, respectively, which is consistent with the cyclic voltammetry (CV) for Pt(111) in $HClO_4$ solution, in which the anion does not specifically adsorb, except for the lower oxidation potential region: The onset potential of H adsorption of 0.11 V is lower than experimental one (about 0.4 V (RHE)).[78] This disagreement mainly stems from a omission of the configurational entropy $k_BT \ln [\theta_H / (1-\theta_H)]$ in the Gibbs energy and errors in the binding energy for the H-Pt bond by the GGA-RPBE functional. These trends are also seen in the past theoretical results.[79, 80]

In the presence of sulfuric acid anions, bisulfate with the surface coverage of $\theta_S$ = 1/10 ML is stable in $0.41 < U \le 0.48$ V, but within the narrow free energy range of about $-0.01 < \Delta G_I \le 0.02$ eV there are three other surface states, sulfate with $\theta_S$ = 1/10 ML, hydronium-sulfate ion pair with $\theta_S$ = 1/10 ML, and coadsorbed bisulfate and hydronium-sulfate ion pair with $\theta_S$ = 1/5 ML. In the higher potential range of $0.48 \text{ V} < U$, sulfate with $\theta_S$ = 1/10 and 1/5 ML is stable. This means that when the electrode potential is increased from a low potential [e.g., $U$ = 0.20 V] in the presence of sulfuric acid, anion adsorption starts at $U \approx 0.4$ V. At the initial stage of the adsorption, bisulfate is the main adsorbate, but sulfate and hydronium-sulfate ion pair also can coadsorb due to the small free energy differences. As the potential becomes higher, bisulfate and hydronium-sulfate ion pair gradually disappear and sulfate becomes the main adsorbate.

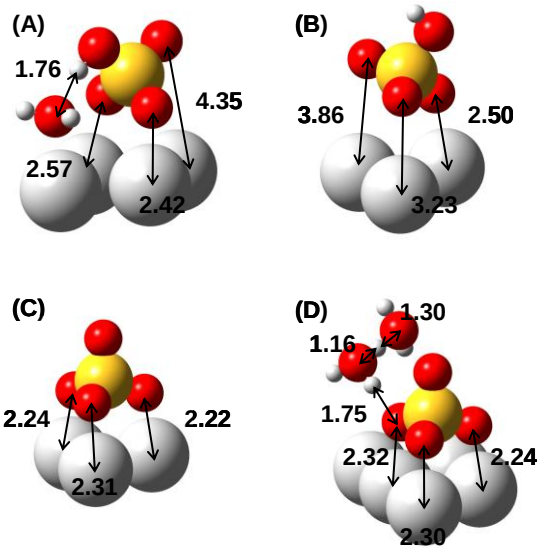


**Fig. 5** Local structures of adsorbed anions; (A) and (B) bisulfate (at 0.43 V (RHE)), (C) sulfate (at 0.62 V (RHE)) and (D) hydronium-sulfate ion pair (0.46 V (RHE)). Only atoms near the adsorbed anions are shown in this figure. The unit of the bond length is Å.

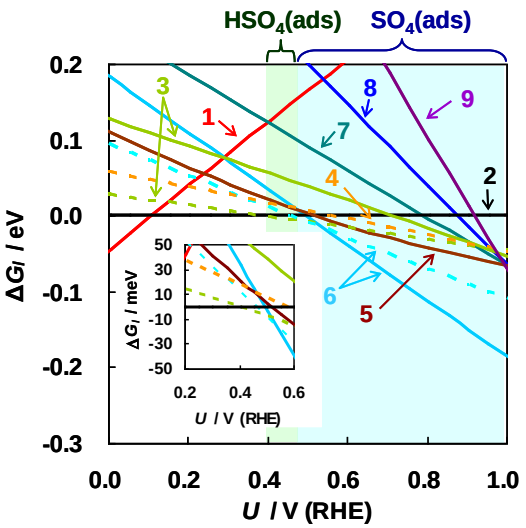


**Fig. 6** Reaction free energies $\Delta G_I$ as functions of the electrode potential $U$. 1 (Red): H(ads); 2 (black): $H_2O$(ads); 3 (light green): bisulfate ($HSO_4$(ads)); 4 (orange): hydronium-sulfate ion pair ($H_3O$-$SO_4$(ads)); 5 (brown): mixture of $HSO_4$(ads) and $H_3O$-$SO_4$(ads); 6 (light blue): sulfate ($SO_4$(ads)); 7 (green): OH(ads); 8 (blue): O(ads) at 1/3 ML; 9 (purple): O(ads) at 1/2 ML. Dashed and solid lines for surfaces with sulfuric acid anions are results for the surface coverage of $\theta_S$ = 1/10 and 1/5 ML, respectively. The inset shows a magnified graph in $0.2 \le U \le 0.6$ V (RHE).

Because the free energy of sulfate is lower than those of OH(asd) and O(ads), sulfate suppresses hydroxide adsorption and oxide formation.

It has been reported that on Pt(111) in $H_2SO_4$ solution, sulfuric acid anion adsorption begins at 0.3 V (RHE),[2–7, 81] and the oxide formation potential is positively shifted from that in $HClO_4$ solution.[3, 11] The calculated results are in good agreement with the experimental results. Our result also agrees with theoretical suggestion that the hydroxide is formed only at domain walls of the $\sqrt{3}\times\sqrt{7}$ structure.[82]

Our conclusion on the preferential adsorbates agrees with the theoretical suggestion by Santana, et al,[36] but is quantitatively different (the hydronium-sulfate ion pair is less stable in our theory).

### 3.3 Electrosorption valency

To check the validity of our calculation further, electrosorption valency $\gamma$ and the total charge density of each adsorbed anion were calculated and compared with the experimentally measured values.

The electrosorption valency can be obtained from two partial derivatives on the basis of cross differentiations of an electrocapillary equation as follows[83, 84]

$$\gamma = \frac{1}{e}\frac{\partial G}{\partial U}\bigg|_{T,p,\theta_S} = -\frac{1}{e}\frac{\partial \sigma}{\partial \theta_S}\bigg|_{T,p,U} . \qquad (28)$$

The partial derivative of the Gibbs free energy with respect to the electrode potential is obtained from the slope of the line shown in Fig. 6 as follows,

$$\gamma = \frac{1}{e}\frac{\partial G}{\partial U}\bigg|_{T,p,\theta_S} = \frac{1}{e\theta_S}\frac{\partial \Delta G_l}{\partial U} . \qquad (29)$$

By this method, the electrosorption valencies are given as –0.7 to –1.2 for bisulfate, hydronium-sulfate ion pair and the mixture of these two species, and –1.9 to –2.1 for sulfate.

The partial derivative of the surface charge with respect to the surface coverage can be also approximately obtained by our theory as follows,

$$\gamma = -\frac{1}{e}\frac{\partial \sigma}{\partial \theta_S}\bigg|_{T,p,U} = -\frac{\partial\left(\int \Delta N_l \frac{d\theta_l}{dt} dt\right)}{\partial\left(\int \frac{d\theta_l}{dt} dt\right)}\bigg|_{T,p,U} \approx -\Delta N_i , \qquad (30)$$

where $\Delta N_l$ is the number of electrons transferred by adsorption per sulfur atom. The calculated $-\Delta N_l$ is shown in Fig. 7 as functions of the electrode potential $U$. $-\Delta N_l$ is –0.4 to –1.2 e for bisulfate, hydronium-sulfate ion pair and the mixture of these two species, while it is –1.7 to –2.1 e for sulfate. The results are consistent with the results given by eqn (29).

Since the dominant adsorbed anion is bisulfate in $0.41 < U \leq 0.48$ V and sulfate in $0.48\ \text{V} < U$ as shown in the section 3.2, $\gamma$ is predicted to be –0.45 to –0.95 at $0.41 < U < 0.48$ V and –1.75 to –1.85 at $U > 0.48$ V. The calculated values are in good agreement with experiments (–0.6 to –1.2 in $0.35 < U \leq 0.50$ V (RHE) and –1.5 to –1.8 in $0.55 < U \leq 0.85$ V (RHE)).[11]

From the result on $\Delta N_l$, the total charge transferred for the formation of the full-coverage-adlayer is calculated to be 90 $\mu C \cdot cm^{-2}$ for sulfate and 45 $\mu C \cdot cm^{-2}$ for bisulfate and hydronium-sulfate ion pair. The former value agrees with an experimental result of about 80 $\mu C \cdot cm^{-2}$,[3, 11] suggesting that sulfate is the major adsorbate.

In CVs for Pt(111) in sulfuric acid, a characteristic sharp current spike superposed on a broad wave is observed at 0.42 V. Santana et al.[36] ascribed to the deprotonation reaction of bisulfate to yield hydronium-sulfate ion pair because the estimated charge

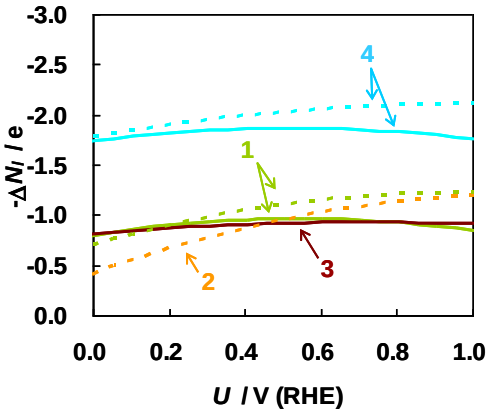


**Fig. 7** The numbers of transferred electrons $\Delta N_l$ through the adsorption of the sulfuric acid anion; 1 (light green): bisulfate ($HSO_4$(ads)); 2 (orange): hydronium-sulfate ion pair ($H_3O$-$SO_4$(ads)); 3 (brown): mixture of $HSO_4$(ads) and $H_3O$-$SO_4$(ads); 4 (light blue): sulfate ($SO_4$(ads)). Dashed and solid lines are results for the surface coverage of $\theta_S$ = 1/10 and 1/5 ML, respectively.

for the deprotonation was close to the experiment values of 8 $\mu C \cdot cm^{-2}$.[81] However, it is worth noting that they estimated the charge from the number of electrons only for surface Pt atoms to which sulfate attached. For a comparison with the experimental data, it should be estimated using the whole cluster atoms.[85] Our estimation of the charge for the deprotonation reaction is –1.9 $\mu C \cdot cm^{-2}$ and does not agree with the experiment. Therefore, the sharp current spike does not stem from the deprotonation and more likely stem from the charge transfer based on the increase in the surface coverage of sulfate associated with the order-disorder phase transition.[8, 9] For exactly clarifying the origin of the sharp current spike, a large scale statistical simulation, such as kinetic Monte Carlo methods, are necessary for estimating the change in the configurational entropy caused by the phase transition. The simulations were already carried out in several publications,[82, 86] and the issue is out of the scope of this study.

## 4 Results and discussion: vibration frequencies

Infrared spectroscopy is a useful way to identify the adsorbate. The infrared spectra reported in the literature are essentially identical. However, the assignments of the observed bands at 1280-1200 and 950 $cm^{-1}$ have been the source of controversy as mentioned in Introduction. We will discuss the band assignment on the basis of the first principles calculation in the following subsections.

### 4.1 Preliminary calculations on clusters

It is known that vibrational frequencies are affected by the theory and basis set used for the calculation. Before discussing results on the extended slab surfaces, the effects of the theory and basis set is discussed. The results obtained from preliminary calculations for $D_2SO_4$, $SO_4^{2-}(H_2O)_3$ and sulfuric acid anions on small Pt clusters are summarized below. All the numerical data are tabulated in Supplementary Information (Section D).

(1) The calculation of the vibration frequencies with different basis sets for $D_2SO_4$ in vacuum (Table S2) revealed that smaller sizes of the basis set (from the aug-cc-pVQZ to the aug-cc-pVDZ) underestimate in a larger extent and the

addition of the second polarization and an f-orbital to the DZP basis set for sulfur reduces the error.

(2) Calculation for a $SO_4^{2-}(H_2O)_3$ cluster in vacuum with various theories and a comparison with the experimental data (Table S3) revealed that GGA-PBE and GGA-RPBE largely underestimate the vibration frequencies, especially for the symmetric and asymmetric S-O stretching frequencies. The smallest error was obtained by using the *ab initio* molecular orbital theory (MP2). The same trend was also reported in the past theoretical studies on various sulfur containing molecules.[87–89]

(3) Comparing with the MP2 results, GGA-PBE and GGA-RPBE calculations result in lower vibration frequencies of sulfate on a $Pt_3$ cluster (Table S4) and bisulfate on a $Pt_2$ cluster (Table S5) in vacuum, the frequencies of which are similar to those on the Pt(111) slab in vacuum (Tables S6 and S7).

(4) The difference between the results obtained by partial Hessian and full Hessian matrices is small (<5 $cm^{-1}$) (Tables S3, S4 and S5).

Although MP2 gives the best prediction, the computational cost of calculations are too high to apply them to the extended slabs in the modeled continuum electrolyte. On the other hand, the cost-effective semi-local exchange-correlation functionals of GGA-PBE and GGA-RPBE underestimate vibration frequencies due to the lack of the non-local contributions on the exchange-correlation interactions among electrons. To make a balance between the cost and accuracy, we make an assumption that the same width of underestimation as in cluster calculations with MP2 and GGA-PBE is generated in the calculation with the modeled continuum electrolyte, and the results by GGA-PBE in the following section are corrected by using the frequency difference between MP2 and GGA-PBE calculations on the clusters as,

$$\nu_{comp} = \nu_{\text{GGA-PBE}}[\text{slab}] + \{\nu_{\text{MP2}}[\text{cluster}] - \nu_{\text{GGA-PBE}}[\text{cluster}]\}. \qquad (31)$$

### 4.2 Vibration frequencies of adsorbates

The vibration frequencies in the range of 800-1400 $cm^{-1}$ for sulfate, bisulfate and hydronium-sulfate ion pair on the Pt(111) surface in the modeled continuum electrolyte were compiled in Table 1. Displacement vectors of each vibrational mode were displayed in Supplementary Information (Section E). The vibration frequencies of bisulfate and sulfate-hydronium ion pair obtained by GGA-PBE (uncorrected values) are close to those obtained by Santana et al.[36] These agreements, however, do not support the assignment by Santana et al. to bisulfate or hydronium-sulfate ion pair[36] because of the underestimation described above. Rather, the frequencies for $\nu_4$ and $\nu_1$ modes of sulfate after compensating the underestimation through eqn (31) are in the best agreement with the experimentally observed frequencies of 1250 and 950 $cm^{-1}$.[12–21]

For better understanding, the results are displayed as spectra in Fig. 8, which were obtained by using calculated dynamic dipole moments perpendicular to the surface (in order to take into account the surface selection rule of surface infrared spectroscopy). As is evident from the figure, only sulfate has a strong band at 1250 $cm^{-1}$ and a weak band at 950 $cm^{-1}$ in consistent with experiments, while the spectra of bisulfate and hydronium-sulfate ion pair are far from the observed spectra. The 1250-$cm^{-1}$ band of sulfate is assigned to the S–O (uncoordinated) stretching mode, while the 950-$cm^{-1}$ band is approximately assigned to the totally symmetric S-O stretching mode. The latter mode is infrared inactive for free sulfate ion ($T_d$ symmetry) but becomes active by the adsorption owing to the symmetry reduction to pseudo-$C_{3v}$. The symmetry reduction also splits the triply degenerate S–O stretching modes at 1104 $cm^{-1}$ for free sulfate ion[13, 90, 91] into three separate modes at 1250, 1020, and 997 $cm^{-1}$. The dynamic dipole moments of the latter two modes are nearly parallel to the surface (Fig. S1), and hence they give only weak absorption in the surface spectra due to the surface selection rule.

**Table 1** Frequencies of sulfate, bisulfate and hydronium-sulfate ion pair on Pt(111) in the modeled continuum electrolyte. Values in the parenthesis are corrected data through eqn (31). The unit is $cm^{-1}$.

| | $\nu_1$ | $\nu_2$ | $\nu_3$ | $\nu_4$ | |
|---|---|---|---|---|---|
| Sulfate at 0.63 V (RHE) | 826 (937) | 866 (997) | 889 (1020) | 1148 (1269) | |
| | $\nu_5$ | $\nu_6$ | $\nu_7$ | $\nu_8$ | $\nu_9$ |
| Hydronium-sulfate ion pair at 0.46 V (RHE) | 822 (933) | 887 (1018) | 1000 (1131) | 986 (1107) | 1310 |
| Hydronium-sulfate ion pair at 0.60 V (RHE) given by Santana et al. (Ref. 36) | – | – | 1014 | – | 1314 |
| | $\nu_{10}$ | $\nu_{11}$ | $\nu_{12}$ | $\nu_{13}$ | |
| Bisulfate in structure at 0.50 V (RHE) | 909 (1014) | 1053 (1173) | 1096 (1148) | 1189 (1288) | |
| Bisulfate at 0.40 V (RHE) given by Santana et al. (Ref. 36) | 866 | 967 | 1128 | 1220 | |

Potential dependence of the frequencies also supports sulfate. Figure 9 shows our theoretical results. The highest frequency for sulfate strongly depends on the electrode potential $U$ (a slope of 58 $cm^{-1}\cdot V^{-1}$), while the remaining three do not (a slope of –20 $cm^{-1}\cdot V^{-1}$). The trend is similar to that observed in the experiments (the slope is 58–130 $cm^{-1}\cdot V^{-1}$ for the highest frequency[5, 18–20] and 0 $cm^{-1}\cdot V^{-1}$ for the lowest frequency[18]). The same analysis showed that the potential dependences of the highest frequencies of

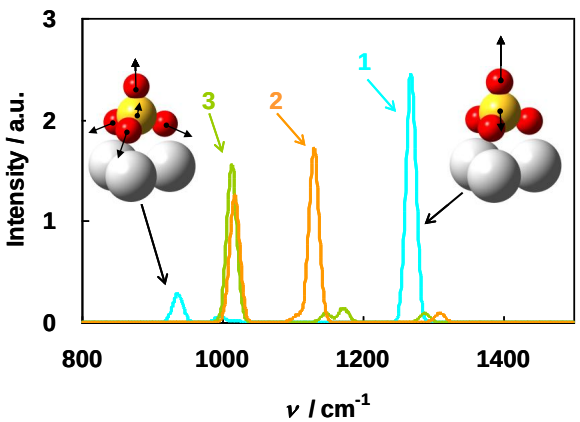


**Fig. 8** Simulated IR spectra; 1 (light blue): sulfate ($SO_4$(ads)); 2 (orange): hydronium-sulfate ion pair ($H_3O$-$SO_4$(ads)); 3 (light green): bisulfate ($HSO_4$(ads)). The intensity was calculated using the Gaussian functions with the frequency width of 10 $cm^{-1}$ centered at the theoretical frequencies. The heights of the Gaussian functions correspond to the squares of the dipole moments along the surface normal. Insets in the graph show the displacement vectors of two IRA active frequencies of sulfate.

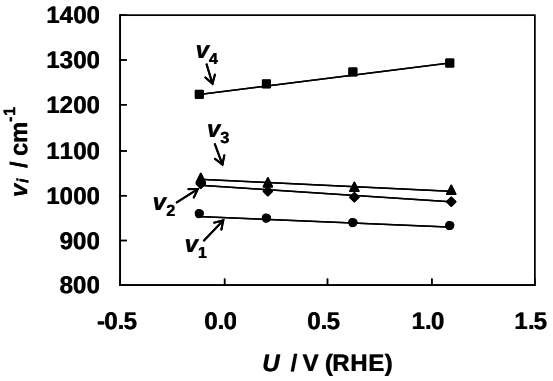


**Fig. 9** Frequencies of sulfate on Pt(111); $\nu_4$ (squares), $\nu_3$ (triangles) and $\nu_2$ (diamonds): asymmetric S-O stretching vibrations; $\nu_1$ (circles): a symmetric S-O stretching vibration. Compensated results through eqn (31) are shown in this figure.

bisulfate and hydronium-sulfate ion pair are –2 and –82 $cm^{-1}\cdot V^{-1}$, respectively, which disagree with the experiments.

## 5. Results and discussion: Double layer structure

Figures 10 (A), (B), (C) and (D) show the effective excess charges per sulfate respectively for $SO_4$, $H_2O$(ads), Pt and the net surface calculated by the Mulliken population analysis[92] on surfaces before (○) and after (●) the adsorption of full coverage sulfate. (The net surface means the sum of $H_2O$(ads) and Pt for the surface before the reaction, and the sum of $SO_4$, $H_2O$(ads) and Pt for the surface after the reaction.) The normalization of the excess charges with respect to sulfate gives the effective charges of one $SO_4$, two $H_2O$(ads), and twenty Pt from the bottom to the top layer of the slab.

Before the adsorption reaction, as shown in Fig. 10 (D), the excess charge for the net surface is zero at $U$ = 0.54 V, i.e., the potential of zero charge (pzc) for the bare Pt(111) surface is 0.54 V. When the potential is increased from the pzc, the excess charge of the net surface increases with the slope of 15 $\mu F\cdot cm^{-2}$, which corresponds to the double-layer capacitance of the bare Pt(111) surface. In all the potential range, the Pt is negatively

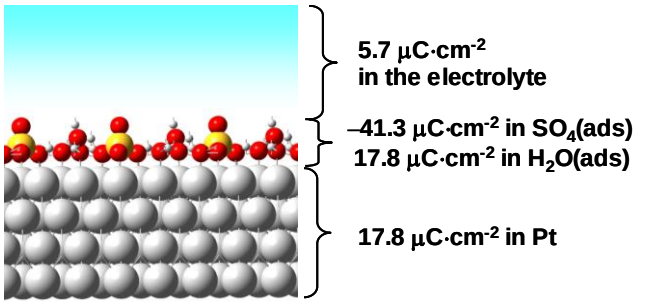


**Fig. 11** The double layer structure with the full coverage sulfate adlayer at 0.63 V (RHE).

charged, and $H_2O$(ads) is positively charged. These theoretical results on the pzc and double-layer capacitance reasonably agree with the experiments of $U_{pzc} \approx 0.3$ V[93, 94] and $C_{dl} = 20$ $\mu F\cdot cm^{-2}$.[95]

By the adsorption, the excess charge for the net surface is decreased by about 0.2 e per sulfate, and becomes negative. This change mainly stems from the negative charge of $SO_4$(ads), which releases electrons by the adsorption, but still has a large negative charge of about –1 e. Both the excess charges of Pt and $H_2O$(ads) become positive and partially cancel the negative charge of $SO_4$(ads). Our result on the charge distribution is similar to that obtained by a distance tunneling spectroscopy combined with DFT calculations on sulfuric acid anion on Au(111),[96, 97] while hydronium ion instead of $H_2O$(ads) is co-adsorbed with sulfate and screens the negative charge of $SO_4$(ads) in the case of Au(111).

On the basis of these theoretical results, the double layer structure of the sulfate adlayer at $U$ = 0.63 V is sketched in Fig. 11. The electrolyte near the surface is positively charged and cancels the surface charge which is negative in this condition, and hence a strong electric field acts on the sulfate. This strong electric field significantly lowers the vibration frequency of the highest asymmetric S-O stretching vibration frequency from 1361 $cm^{-1}$ in vacuum (see the data by MP2 in Table S4) to 1269$cm^{-1}$ in the modeled electrolyte (see the corrected data in Table 1). By increasing the potential, the surface excess charge approaches to zero as shown in Fig. 10 (D), and the electric field becomes small. Therefore, the band is blue shifted as shown in Fig. 9.

Finally, by using the results on the charge distribution,

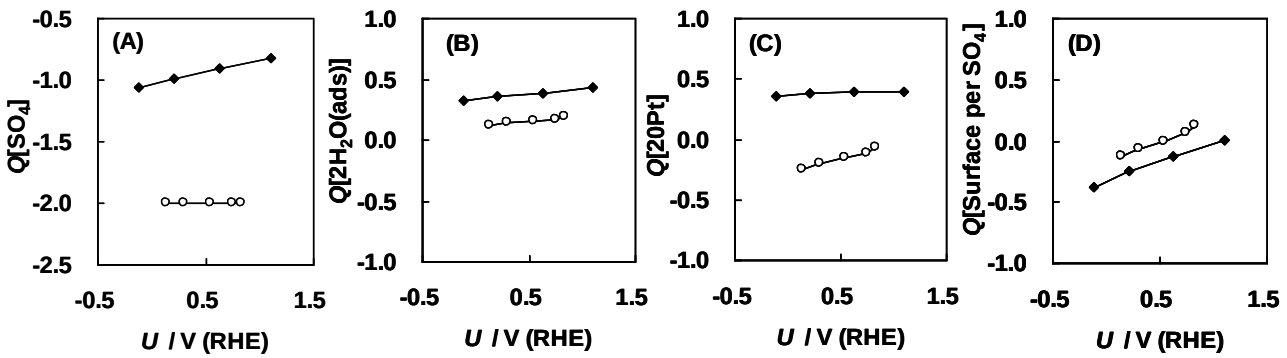


**Fig. 10** Excess effective charges before and after the adsorption of the full coverage sulfate; (A) $SO_4$; (B) $H_2O$(ads); (C) Pt; (D) the net surface. Open and black circles are results respectively for systems before and after the adsorption reaction.

the adsorption of the sulfuric acid anion on the Pt(111) surface at $U$ = 0.63 V is described as an oxidation reaction:

$$\mathrm{HSO_4^-(aq)+(2H_2O)^{0.16}(ads)+(5Pt)^{-0.14}} \rightarrow \mathrm{SO_4^{-0.91}(ads)+(2H_2O)^{0.39}(ads)+(5Pt)^{0.39}+H^+(aq)+1.85e^-}, \quad (32)$$

where the Pt in this equation indicates the surface Pt atoms.

## 6. Conclusion

A first principles theory combined with a continuum electrolyte theory[29, 35] was applied to the specific adsorption of sulfuric acid anions on Pt(111) surface. Results are summarized as follows:

(i) The free energy diagram indicates that sulfuric acid anions adsorb as bisulfate in $0.41 < U \leq 0.48$ V and sulfate in 0.48 V $< U$.

(ii) The total transferred charge through the formation of the full coverage sulfate adlayer is 90 $\mu C \cdot cm^{-2}$.

(iii) The electrosorption valency is estimated to be −0.45 to −0.95 in $0.41 < U \leq 0.48$ V and −1.75 to −1.85 in 0.48 V $< U$. This transition stems from the change in the preferential form of the adsorbed anion from bisulfate in the lower potential range to sulfate in the higher potential range.

(iv) The observed vibrational frequencies at 1250 and 950 $cm^{-1}$ can be assigned respectively to the S-O (uncoordinated) and symmetric S-O stretching modes for the sulfate. The higher frequency has a larger potential-dependence with a slope of 58 $cm^{-1} \cdot V^{-1}$ than the lower one.

Our theoretical results are in good agreement with electrochemical and spectroscopic experimental results and firstly provide atomic scale charge distribution in the electric double layer on Pt(111) in sulfuric acid solution. We believe that our methodology can be widely applied to various ion-metal interacting systems including other oxyanion, halide anion, cation and ionomer in actual fuel cells.

## References


1 W. Grove, *Philos. Mag., Ser. 3*, 1839, **14**, 127.
2 J. Clavilier, *J. Electroanal. Chem.*, 1980, **107**, 211.
3 N. M. Marković, B. N. Grgur, C. A. Lucas and P. N. Ross, *J. Phys. Chem. B*, 1999, **103**, 487.
4 E. Herrero, J. Mostany, J. M. Feliu and J. Lipkowski, *J. Electroanal. Chem.*, 2002, **534**, 79.
5 V. Climent, N. Carcía-Araez and J. M. Feliu, *Electrochem. Comm*, 2006, **8**, 1577.
6 N. Garcia-Araez, V. Climent, P. Rodriguez and J. M. Feliu, *Electrochim. Acta*, 2008, **53**, 6793.
7 N. Garcia-Araez, V. Climent, P. Rodriguez and J. M. Feliu, *Phys. Chem. Chem. Phys.*, 2010, **12**, 12146.
8 A. M. Funtikov, U. Linke, U. Stimming and R. Vogel, *Surf. Sci.*, 1995, **324**, L343.
9 L. –J. Wan, S. –L. Yau and K. Itaya, *J. Phys. Chem*, 1995, **99**, 9507.
10 B. Braunschweig and W. Daum, *Langmuir*, 2009, **25**, 11112.
11 A. Kolics and A. Wieckowski, *J. Phys. Chem. B*, 2001, **105**, 2588.
12 P. W. Faguy, N. Marković, R. R. Azdic, C. A. Fierro and E. B. Yeager, *J. Electroanal. Chem.*, 1990, **289**, 245.
13 R. J. Nichols, In:*Adsorption of Molecules at Metal Electrodes*, J. Lipkowski and P. N. Ross, Eds., VCH Publishers: New York, 1992, p347.
14 Y. Sawatari, J. Inukai and M. Ito, *J. Electron Spectrosc.*, 1993, **64-65**, 515.
15 F. C. Nart, T. Iwashita and M. Weber, *Electrochim. Acta*, 1994, **39**, 961.
16 P. W. Faguy, S. Marinkovic and R. R. Adzic, *J. Electroanal. Chem.*, 1996, **407**, 209.
17 Y. Shingaya and M. Ito, *Chem. Phys. Lett.*, 1996, **256**, 438.
18 A. Lanchenwitzer, N. Li and J. Lipkowski, *J. Electroanal. Chem.*, 2002, **532**, 85.
19 N. Hoshi, M. Kuroda, O. Koga and Y. Hori, *J. Phys. Chem. B*, 2002, **106**, 9107.
20 B. Braunschweig, P. Mukherjee, D. D. Dlott and A. Wieckowski, *J. Am. Chem. Soc.*, 2010, **132**, 14036.
21 Z. Su, V. Climent, J. Leitch, V. Zamlynny, J. M. Feliu and J. Lipkowski, *Phys. Chem. Chem. Phys.*, 2010, **12**, 15231.
22 P. Hohenberg and W. Kohn, *Phys. Rev.*, 1964, **136**, B864.
23 W. Kohn and L. J. Sham., *Phys. Rev.*, 1965, **140**, A1133.
24 A. B. Anderson and T. V. Albu, *J. Am. Chem. Soc.*, 1999, **121**, 11855.
25 C. D. Taylor, S. A. Wasileski, J. –S. Filhol and M. Neurock, *Phys. Rev. B: Condens. Matter Mater. Phys.*, 2006, **73**, 165402.
26 M. Otani and O. Sugino, *Phys. Rev. B: Condens. Matter Mater. Phys.*, 2006, **73**, 115407.
27 E. Skúlason, G. Karlberg, J. Rossmeisl, T. Bligaard, J. Greeley, H. Jónsson and J. K. Nørskov, *Phys. Chem. Chem. Phys.*, 2007, **9**, 3241.
28 Y. Ishikawa, J. J. Mateo, D. A. Tryk and C. R. Cabrera, *J. Electroanal. Chem.*, 2007, **607**, 37.
29 R. Jinnouchi and A. B. Anderson, *Phys. Rev. B: Condens. Matter Mater. Phys.*, 2008, **77**, 245417.
30 A. B. Anderson and T. V. Albu, *J. Electrochem. Soc.*, 2000, **147**, 4229.
31 D. Cao, G. –Q. Lu, A. Wieckowski, S. A. Wasileski and M. Neurock, *J. Phys. Chem. B*, 2005, **109**, 11622.
32 M. Otani, I. Hamada, O. Sugino, Y. Morikawa, Y. Okamoto and T. Ikeshoji, *Phys. Chem. Chem. Phys.*, 2008, **10**, 3609.
33 R. Jinnouchi and A. B. Anderson, *J. Phys. Chem.* C, 2008, **112**, 8747.
34 V. Tripković, E. Skúlason, S. Siahrostami, J. K. Nørskov and J. Rossmeisl, *Electrochim. Acta*, 2010, **55**, 7975.
35 R. Jinnouchi, K. Kodama, T. Hatanaka and Y. Morimoto, *Phys. Chem. Chem. Phys.*, 2011, **13**, 21070.
36 J. Santana, C. R. Cabrera and Y. Ishikawa, *Phys. Chem. Chem. Phys.*, 2010, **12**, 9526.
37 A. J. Bard, R. Parsons and J. Jordan, *Standard Potentials in Aqueous Solution*, Marcel Dekker, New York, 1985.
38 J. Tomasi and M. Persico, *Chem. Rev.*, 1994, **94**, 2027.
39 S. Miertuš, E. Scrocco and J. Tomasi, *Chem. Phys.*, 1981, **55**, 117.
40 M. Cossi, V. Barone, R. Cammi and J. Tomasi, *Chem. Phys. Lett.*, 1996, **327**, 255.
41 A. Klamt and G. Schüürmann, J. Chem. Soc., Perkin trans., 1993, **2**, 799.
42 C. J. Cramer and D. G. Truhlar, *J. Am. Chem. Soc.*, 1991, **113**, 8305.
43 D. A. Scherlis, J.-L. Fattebert, G. Gygi, M. Cococcioni and N. Marzari, *J. Chem. Phys.*, 2006, **124**, 074103.
44 V. M. Sánchez, M. Sued and D. A. Scherlis, *J. Chem. Phys.*, 2009, **131**, 174108.
45 Y.-H. Fang and Z.-P. Liu, *J. Am. Chem. Soc.*, 2010, **132**, 18214.
46 I. Borukhov, D. Andelman and H. Orland, *Phys. Rev. Lett.*, 1997, **79**, 435.
47 I. Borukhov, D. Andelman and H. Orland, *Electrochim. Acta*, 2000, **46**, 221.
48 J. I. Steinfeld, J. S. Francisco and W. L. Hase, *Chemical Kinetics and Dynamics*, Prentice Hall, Englewood Cliffs, NJ, 1989.
49 R. Cammi, C. Cappelli, S. Corni and J. Tomasi, *J. Phys. Chem. A*, 2000, **104**, 9874.
50 C. Cappelli, F. Lipparini, J. Bloino and V. Barone, *J. Chem. Phys.*, 2011, **135**, 104505.
51 P. S. Bagus, C. J. Nelin, W. Müller, M. R. Philpott and H. Seki, *Phys. Rev. Lett.*, 1987, **58**, 559.
52 S. A. Wasileski, M. T. M. Koper and M. J. Weaver, J. Am. Chem. Soc., 2002, **124,** 2796.
53 M. Tomonari and O. Sugino, *Chem. Phys. Lett.*, 2007, **437**, 170.
54 CRC Handbook of Chemistry and Physics, 49th ed., R. C. Weast, Ed., The Chemical Rubber Company: Cleveland, OH, 1968-1969: p. D109.

55 G. J. Tawa, I. A. Topol, S. K. Burt, R. A. Caldwell and A. A. Rashin, *J. Chem. Phys.*, 1998, **109**, 4852.
56 M. D. Tissandier, K. A. Cowen, W. Y. Feng, E. Gundlach, M. H. Cohen, A. D. Earhart, J. V. Coe and T. R. Tuttle Jr., *J. Phys. Chem. A*, 1998, **102**, 7787.
57 J. O. M. Bockris, M. Gamboa-Aldeco and M. Szklarczyk, *J. Electroanal. Chem.*, 1992, **339**, 355.
58 D. L. Doering and T. E. Madey, *Surf. Sci.*, 1982, **123**, 305.
59 H. Ogasawara, B. Brena, D. Nordlund, M. Nyberg, A. Pelmenschikov, L. G. M. Pettersson and A. Nilsson, *Phys. Rev. Lett.*, 2002, **89**, 276102.
60 A. Michaelides, A. Alavi and D. A. King, *Phys. Rev. B: Condens. Matter Mater. Phys.*, 2004, **69**, 113404.
61 C. Clay, S. Haq and A. Hodgson, *Phys. Rev. Lett.*, 2004, **92**, 046102.
62 G. S. Karlberg and G. Wahnström, *Phys. Rev. Lett.*, 2004, **92**, 136103.
63 G. S. Karlberg and G. Wahnström, *J. Chem. Phys.*, 2005, **122**, 194705.
64 B. Hammer, L. B. Hansen and J. K. Nørskov, *Phys. Rev. B: Condens. Matter Mater. Phys.*, 1999, **59**, 7413.
65 J. P. Perdew, K. Burke and M. Ernzerhof, *Phys. Rev. Lett.*, 1996, **77**, 3865.
66 J. D. Pack and H. J. Monkhorst, *Phys. Rev. B: Condens. Matter Mater. Phys.*, 1976, **13**, 5188.
67 C. –L. Fu and K. –M. Ho, *Phys. Rev. B: Condens. Matter Mater. Phys.*, 1983, **28**, 5480.
68 J. –L. Fattebert and F. Gygi, *J. Comp. Chem.*, 2002, **23**, 662.
69 J. –L. Fattebert and F. Gygi, *Int. J. Quantum Chem.*, 2003, **93**, 139.
70 Gaussian 03, Revision C.02, M. J. Frisch, G. W. Trucks, H. B. Schlegel, G. E. Scuseria, M. A. Robb, J. R. Cheeseman, J. A. Montgomery, Jr., T. Vreven, K. N. Kudin, J. C. Burant, J. M. Millam, S. S. Iyengar, J. Tomasi, V. Barone, B. Mennucci, M. Cossi, G. Scalmani, N. Rega, G. A. Petersson, H. Nakatsuji, M. Hada, M. Ehara, K. Toyota, R. Fukuda, J. Hasegawa, M. Ishida, T. Nakajima, Y. Honda, O. Kitao, H. Nakai, M. Klene, X. Li, J. E. Knox, H. P. Hratchian, J. B. Cross, V. Bakken, C. Adamo, J. Jaramillo, R. Gomperts, R. E. Stratmann, O. Yazyev, A. J. Austin, R. Cammi, C. Pomelli, J. W. Ochterski, P. Y. Ayala, K. Morokuma, G. A. Voth, P. Salvador, J. J. Dannenberg, V. G. Zakrzewski, S. Dapprich, A. D. Daniels, M. C. Strain, O. Farkas, D. K. Malick, A. D. Rabuck, K. Raghavachari, J. B. Foresman, J. V. Ortiz, Q. Cui, A. G. Baboul, S. Clifford, J. Cioslowski, B. B. Stefanov, G. Liu, A. Liashenko, P. Piskorz, I. Komaromi, R. L. Martin, D. J. Fox, T. Keith, M. A. Al-Laham, C. Y. Peng, A. Nanayakkara, M. Challacombe, P. M. W. Gill, B. Johnson, W. Chen, M. W. Wong, C. Gonzalez and J. A. Pople, Gaussian, Inc., Wallingford CT, 2004.
71 A. D. Becke, *J. Chem. Phys.*, 1993, **98**, 5648.
72 A. Szabo and N. Ostlund, *Modern Quantum Chemistry: Introduction to Advanced Electronic Structure Theory*, Dover, 1996.
73 R. Krishnan, J. S. Binkley, R. Seeger and J. A. Pople, *J. Chem. Phys.*, 1980, **72**, 650.
74 P. J. Hay and W. R. Wadt, *J. Chem. Phys.*, 1985, **82**, 270.
75 T. H. Dunning Jr., *J. Chem. Phys.*, 1989, **90**, 1007.
76 R. A. Kendaal, T. H. Dunning Jr. and R. J. Harrison, *J. Chem. Phys.*, 1992, **96**, 6796.
77 D. E. Woon and T. H. Dunning Jr., *J. Chem. Phys.*, 1993, **98**, 1358.
78 N. M. Marković and P. N. Ross, *Surf. Sci. Rep.*, 2002, **45**, 117.
79 J. Rossmeisl, J. K. Nørskov, C. D. Taylor, M. J. Janik and M. Neurock, *J. Phys. Chem. B*, 2006, **110**, 21833.
80 G. S. Karlberg, T. F. Jaramillo, E. Skúlason, J. Rossmeisl, T. Bligaard and J. K. Nørskov, *Phys. Rev. Lett.*, 2007, **99**, 126101.
81 N. García, V. Climent, J. M. Orts, J. M. Feliu and A. Aldaz, *ChemPhysChem*, 2004, **5**, 1221.
82 C. Saravanan, M. T. M. Koper, N. M. Markovic, M. Head-Gordon and P. N. Ross, *Phys. Chem. Chem. Phys.*, 2002, **4**, 2660.
83 S. Trasatti and R. Parsons, *J. Electroanal. Chem.*, 1986, 205, 359.
84 W. Schmickler and E. Santos, *Interfacial Electrochemistry*, *2nd Edition*, Springer, 1996.
85 For example, for the formation of the full coverage adlayer, the analysis using the number of electrons in the Pt atoms attached to sulfate shown in Santana's work gives a much smaller charge (7 $\mu C \cdot cm^{-2}$) than the experiments (80 $\mu C \cdot cm^{-2}$). In contrast, our model using the number of electrons in the whole slab gives a charge (90 $\mu C \cdot cm^{-2}$) closer to the experiments.
86 P. A. Rikvold, M. Gamboa-Aldeco, J. Zhang, M. Han, Q. Wang, H. L. Richards and A. Wieckowski, *Surf. Sci.*, 1995, **335**, 389.
87 J. Zhoh, G. Santambrogio, M. Brümmer, D. T. Moore, L. Wöste, G. Meijer, D. M. Neumark and K. R. Asmis, *J. Chem. Phys.*, 2006, **125**, 111102.
88 J. A. Altmann and N. C. Handy, *Phys. Chem. Chem. Phys.*, 1999, **1**, 5529.
89 G. Menconi and D. J. Tozer, *Phys. Chem. Chem. Phys.*, 2003, **5**, 2938.
90 P. W. Faguy, N. S. Marinkovic and R. R. Adzic, *Langmuir*, 1996, **12**, 243.
91 T. Iwasita and F. C. Nart, *Prog. Surf. Sci.*, 1997, **55**, 271.
92 R. S. Mulliken, *J. Chem. Phys.*, 1955, **23**, 1833.
93 J. Clavilier, R. Albalat, R. Gómez, J. M. Ortz, J. M. Feliu and A. Aldaz, *J. Electroanal. Chem.*, 1992, **330**, 489.
94 A. Cuesta, *Surf. Sci.*, 2004, **572**, 11.
95 T. Pajkossy and D. M. Kolb, *Electrochim. Acta*, 2001, **46**, 3063.
96 F. C. Simeone, D. M. Kolb, S. Venkatachalam and T. Jacob, *Angew. Chem. Int. Ed.*, 2007, **46**, 8903.
97 F. C. Simeone, D. M. Kolb, S. Venkatachalam and T. Jacob, *Surf. Sci.*, 2008, **602**, 1401.

**Supplementary information for**

# First principles study of sulfuric acid anion adsorption on Pt(111) electrode

*Ryosuke Jinnouchi,*[†]* *Tatsuya Hatanaka,*[†] *Yu Morimoto*[†] *and Masatoshi Osawa*[‡]

[†]Toyota Central Research & Development Laboratories, Inc., Nagakute, Aichi 480-1192, Japan

[‡]Catalysis Research Center, Hokkaido University, Sapporo 001-0021, Japan

## A. Mean field of static solvation medium

Within the Born-Oppenheimer approximation, a Hamiltonian of an interfacial system is described as follows,

$$H\left[\{\mathbf{P}_i\},\{\mathbf{R}_i\},\{\mathbf{P}_i^m\},\{\mathbf{R}_i^m\}\right]=\sum_i \frac{\left|\mathbf{P}_i\right|^2}{2M_i}+\sum_i \frac{\left|\mathbf{P}_i^m\right|^2}{2M_i^m}+E\left[\{\mathbf{R}_i\},\{\mathbf{R}_i^m\}\right], \tag{A.1}$$

where $\mathbf{P}_i$ and $\mathbf{R}_i$ are momentums and positions of atoms in the region (i), and $E$ is the potential energy of the system. The momentums and positions of atoms in the solvation medium (the region (ii)) are denoted using the superscript $m$. The partition function of the system is described as follows,

$$Q=\frac{1}{\prod_i h^{3N_i}\prod_i h^{3N_i^m}}\int\cdots\int \exp\left[-\frac{H\left[\{\mathbf{P}_i\},\{\mathbf{R}_i\},\{\mathbf{P}_i^m\},\{\mathbf{R}_i^m\}\right]}{k_BT}\right]\prod_i d\mathbf{P}_i d\mathbf{R}_i \prod_i d\mathbf{P}_i^m d\mathbf{R}_i^m , \tag{A.2}$$

where $N_i$ and $N_i^m$ are the numbers of atoms in the region (i) and region (ii), respectively. For simplifying the equation, all the atoms in the system are assumed to be non-identical in this section, but it is straightforward to extend equations to the system including identical atoms.

By using the Hamiltonian of the system without the region (ii) described as,

$$H_0\left[\{\mathbf{P}_i\},\{\mathbf{R}_i\}\right]=\sum_i \frac{\left|\mathbf{P}_i\right|^2}{2M_i}+E_0\left[\{\mathbf{R}_i\}\right], \tag{A.3}$$

eqn (A.2) can be rewritten as follows,

$$Q=\frac{1}{\prod_i h^{3N_i}}\int\cdots\int \exp\left[-\frac{H_0\left[\{\mathbf{P}_i\},\{\mathbf{R}_i\}\right]+G_m\left[\{\mathbf{R}_i\}\right]}{k_BT}\right]\prod_i d\mathbf{P}_i d\mathbf{R}_i , \tag{A.4}$$

where $G_m$ is the mean field (or potential of mean force) of the region (ii) defined as follows,

$$G_m\left[\{\mathbf{R}_i\}\right] = k_B T \ln \frac{1}{\prod_i h^{3N_i^m}} \int \cdots \int \exp\left[ - \frac{\sum_i \frac{\left|\mathbf{P}_i^m\right|^2}{2M_i^m} + E\left[\{\mathbf{R}_i\}, \{\mathbf{R}_i^m\}\right] - E_0\left[\{\mathbf{R}_i\}\right]}{k_B T} \right] d\mathbf{P}_i^m d\mathbf{R}_i^m \ . \qquad \text{(A.5)}$$

On the basis of eqn (A.4), the system can be approximately regarded as the atoms in the region (i) moving on the effective potential energy surface described as follows,

$$E_1\left[\{\mathbf{R}_i\}\right] = E_0\left[\{\mathbf{R}_i\}\right] + G_m\left[\{\mathbf{R}_i\}\right]. \qquad \text{(A.6)}$$

This approximate picture is sometimes called as a static solvation[48] and has been successfully used in the self-consistent reaction field (SCRF) theory on isolated molecules and ions implemented in various well-established computational programs[70] for evaluating not only the static properties like solvation free energies[38–44] but also the dynamic properties like vibration frequencies.[49, 50]

## B. Continuum solvation model

As in the usual DFT,[22, 23] the kinetic and exchange-correlation energies of electrons in the region (i) are described as follows,

$$K = \sum_n f_n \int d\mathbf{r}\, \psi_n^*(\mathbf{r}) \left( -\frac{1}{2}\nabla^2 \right) \psi_n(\mathbf{r}), \tag{B.1}$$

$$E_{xc} = E_{xc}\left[\rho_\uparrow, \rho_\downarrow\right] = \int d\mathbf{r} f_{xc}\left(\rho_\uparrow, \rho_\downarrow, \nabla\rho_\uparrow, \nabla\rho_\downarrow\right), \tag{B.2}$$

where $n$ denotes **k**-point, spin and band indexes, and $\rho_s$ ($s$ = ↑ or ↓) is the electron density with a spin index $s$. In this study, two generalized gradient approximations (GGAs)[64, 65] were applied, and therefore, $E_{xc}$ is described as a functional of the electron densities and those derivatives.

The electrostatic energy $E_{es}$ is described as follows,

$$E_{es} = \int d\mathbf{r}\left[\rho_\uparrow(\mathbf{r}) + \rho_\downarrow(\mathbf{r}) + \rho_c(\mathbf{r}) + \rho_+(\mathbf{r}) + \rho_-(\mathbf{r})\right]\phi(\mathbf{r}) - \int d\mathbf{r} \frac{\varepsilon(\mathbf{r})}{8\pi} \left|\nabla\phi(\mathbf{r})\right|^2 , \tag{B.3}$$

where $\rho_c$ is the charge density of the nuclei in the region (i), and $\varepsilon$ is the dielectric permittivity. Similarly to the polarizable continuum model, $\varepsilon$ is 1 near the atoms in the region (i) and is $\varepsilon_b$ ( = 78.36) far from the atoms. At the intermediate region, $\varepsilon$ smoothly changes from 1 to $\varepsilon_b$. Details of the function form of $\varepsilon$ is described elsewhere.[29]

The non-electrostatic free energy $G_{ss,nes}$ is a summation of cavitation, dispersion and repulsion free energies, which are denoted as $G_{ss,cav}$, $G_{ss,dr}$ and $G_{ss,rep}$. The cavitation free energy $G_{ss,cav}$ is described as a product of a total surface area $S$ of the atoms in the region (i) by a surface tension $\gamma_b$ ( = 71.99 mN/m) of the solvent as follows,

$$G_{ss,cav} = \gamma_b S\,. \tag{B.4}$$

The surface area $S$ is obtained by a methodology[29] similar to that suggested by Scherlis et al.[43] The dispersion and repulsion free energies are obtained as a linear function of atomic surface areas $\{S_\alpha\}$ as follows,

$$G_{ss,dr} + G_{ss,rep} = \sum_\alpha \left( a_\alpha S_\alpha + b_\alpha \right). \tag{B.5}$$

$S_\alpha$ is obtained by partitioning $S$ using a methodology described in Ref. 29. Parameters $a_\alpha$ and $b_\alpha$ were determined to reproduce the dispersion and repulsion free energies of molecules and ions in a homogeneous solution given by the polarizable continuum model implemented in Gaussian03.[70]

The non-electrostatic interaction energy $G_{is,nel}$ is described as follows,

$$G_{is,nel} = \int d\mathbf{r} \left( \left| \rho_-(\mathbf{r}) \right| + \left| \rho_+(\mathbf{r}) \right| \right) \phi_{rep}(\mathbf{r}). \tag{B.6}$$

$\phi_{rep}$ describes non-electrostatic repulsive potentials between atoms in the region (i) and ions in the region (ii). The repulsive interaction avoids that ions in the region (ii) approach to atoms in the region (i) too closely. A similar repulsive potential was introduced by Otani and Sugino[26] for describing a Stern layer, and the methodology was extended to an adaptive form in a variationally consistent manner by Jinnouchi and Anderson.[29]

The entropy $S_i$ is described using a lattice gas model as follows,

$$\begin{aligned} S_i = -\frac{k_B}{a^3} \int d\mathbf{r} [ & \left| \rho_+(\mathbf{r}) \right| a^3 \ln \left( \left| \rho_+(\mathbf{r}) \right| a^3 \right) + \left| \rho_-(\mathbf{r}) \right| a^3 \ln \left( \left| \rho_-(\mathbf{r}) \right| a^3 \right) \\ & + \left( 1 - \left| \rho_+(\mathbf{r}) \right| a^3 - \left| \rho_-(\mathbf{r}) \right| a^3 \right) \ln \left( 1 - \left| \rho_+(\mathbf{r}) \right| a^3 - \left| \rho_-(\mathbf{r}) \right| a^3 \right) ] \end{aligned}. \tag{B.7}$$

This term was introduced by Borukhov et al.[46, 47] to describe steric effects of ion in a solution.

$G_{mc}$ is described as follows,

$$G_{mc} = -\varepsilon_F N - \mu_+ N_+ - \mu_- N_-, \tag{B.8}$$

where $N_{\pm}$ are the numbers of cation and anion:

$$N_{\pm} = \int \rho_{\pm}(\mathbf{r}) d\mathbf{r}, \tag{B.9}$$

The chemical potentials $\mu_{\pm}$ of ions are the same as those in the bulk electrolyte in contact with the system. Those are obtained using a lattice gas model of the bulk electrolyte[46, 47] as follows,

$$\mu_{\pm} = k_B T \ln \frac{c_b a^3}{1 - 2c_b a^3}. \tag{B.10}$$

## C. Enthalpies and entropies of chemical species

Adsorbed species are assumed to be rigidly bounded to the surface, and those enthalpies $H_n$ and entropies $S_n$ based on the motions of nuclei are described using a harmonic oscillator model as follows,

$$H_n = H_{vib} = \frac{1}{2}\sum_i h\nu_i + \sum_i \frac{h\nu_i}{e^{h\nu_i/k_BT}-1}, \tag{C.1}$$

$$S_n = S_{vib} = k_B \sum_i \left( \frac{h\nu_i/k_BT}{e^{h\nu_i/k_BT}-1} - \ln\left(1-e^{-h\nu_i/k_BT}\right)\right), \tag{C.2}$$

where $h$ is the Planck constant, and $\nu_i$ is the frequency of $i$th vibration mode. For the chemical species in a homogeneous gas phase or aqueous phase, translation, rotation, and vibration motions are taken into account as follows,

$$H_n = H_{trans} + H_{rot} + H_{vib}, \tag{C.3}$$

$$S_n = S_{trans} + S_{rot} + S_{vib}, \tag{C.4}$$

$$H_{trans} = \frac{3}{2}k_BT, \tag{C.5}$$

$$H_{rot} = \begin{cases} k_BT, & \text{for linear molecules} \\ \frac{3}{2}k_BT, & \text{for nonlinear molecules} \end{cases}, \tag{C.6}$$

$$S_{trans} = k_B\left( \ln\left( \frac{2\pi m k_BT}{h^2}\right)^{3/2} \frac{k_BT}{p} + 1 + \frac{3}{2}\right), \tag{C.7}$$

$$S_{rot} = \begin{cases} k_B \ln\left( \frac{T}{\sigma\Theta_z} + 1\right), & \text{for linear molecules} \\ k_B \ln\left( \frac{\pi^{1/2}T^{3/2}}{\sigma_{rot}\sqrt{\Theta_x\Theta_y\Theta_z}} + \frac{3}{2}\right), & \text{for nonlinear molecules} \end{cases}, \tag{C.8}$$

$$\Theta_{x,y,z} = \frac{h^2}{8\pi^2 I_{x,y,z} k_B}. \quad \text{(C.9)}$$

where $m$ is the mass of the specie, $p$ is the pressure, $\sigma_{rot}$ is the rotational symmetry number, and $I_{x,y,z}$ are the momentum inertia.

All the enthalpies and entropies are compiled in Table S1.

**Table S1** $H_n$ and $TS_n$ ($T$ = 298.15 K). For species in gas phase, the pressure is set at 1 atm. $H_2O$(aq) corresponds to $H_2O$(g) with a vapor pressure of 0.035 atm. The unit of energy is eV. The data for the adsorbates were obtained by using the partial Hessian matrices.

| | $H_n$ | $TS_n$ |
|---|---|---|
| $H_2O$(aq) | 0.665 | 0.673 |
| $H_2O$(ads) | 0.724 | 0.086 |
| $H^+$(g) | 0.064 | 0.337 |
| $HSO_4^-$(g) | 0.821 | 0.909 |
| $SO_4$(ads)+$H_2O$(ads) | 1.321 | 0.372 |
| $HSO_4$(ads)+$H_2O$(ads) | 1.620 | 0.440 |
| $H_3O$-$SO_4$(ads) | 1.570 | 0.354 |
| H(ads) | 0.141 | 0.016 |
| OH(ads) | 0.400 | 0.130 |
| O(ads) | 0.098 | 0.041 |

## D. Results of preliminary calculations on small clusters

Results of preliminary calculations on small clusters are compiled in Table S2-S7. Details of the calculation method are described in the section 2.6.

As described in the section 4.1, the GGA-PBE results on the extended slabs in the modeled continuum electrolyte shown in the section 4.2 were corrected through eqn (31). In this correction, the results by MP2/6-311++G(2df,2pd) and GGA-PBE/6-311++G(2df,2pd) in Tables S4 and S5 were used.

**Table S2** Frequencies of a $D_2SO_4$ molecule in vacuum. All the calculations were performed by using the GGA-PBE functional. $\Delta\nu$ is the average error from the experimental results. The unit is $cm^{-1}$.

| | $\nu_1$ | $\nu_2$ | $\nu_3$ | $\nu_4$ | $\nu_5$ | $\nu_6$ | $\nu_7$ | $\nu_8$ | $\Delta\nu$ |
|---|---|---|---|---|---|---|---|---|---|
| Exp.[a] | 547 | 565 | 820 | 834 | 883 | 1223 | 1446 | 2663 | – |
| FEM[b] | 509 | 537 | 818 | 835 | 881 | 1164 | 1400 | 2649 | –24 |
| aug-cc-pVQZ[c] | 497 | 507 | 801 | 827 | 873 | 1157 | 1389 | 2656 | –34 |
| aug-cc-pVTZ[c] | 487 | 497 | 791 | 828 | 873 | 1141 | 1370 | 2651 | –43 |
| aug-cc-pVDZ[c] | 464 | 696 | 753 | 828 | 868 | 1084 | 1305 | 2638 | –43 |
| 6-311++G(2df,2pd)[c] | 495 | 506 | 802 | 830 | 875 | 1156 | 1390 | 2666 | –33 |
| DZDP+f[d] | 503 | 507 | 779 | 823 | 863 | 1163 | 1398 | 2662 | –35 |
| DZP[e] | 483 | 491 | 763 | 833 | 870 | 1131 | 1368 | 2665 | –47 |

a. Experimental results from Ref. S1.

b. Theoretical results from Ref. S2 obtained by using a finite-element basis set.

c Theoretical results by Gaussian 03 (Ref. 70).

d Theoretical results by the methodology used in this study.

e Theoretical results by using the basis set without the second polarization and the f-orbital.

**Table S3** Frequencies of a $SO_4^{2-}(H_2O)_3$ cluster in vacuum. $\Delta\nu$ is the average error from the experimental results. Partial hess. means that the frequencies are obtained by using partial Hessian matrices of $SO_4$. The unit is $cm^{-1}$.

| | $\nu_1$ | $\nu_2$ | $\nu_3$ | $\nu_4$ | $\nu_5$ | $\nu_6$ | $\nu_7$ | $\Delta\nu$ |
|---|---|---|---|---|---|---|---|---|
| Exp.[a] | 613 | 862 | 943 | 1052 | 1080 | 1102 | 1735 | – |
| MP2/TZP[b] | 589 | 869 | 913 | 1058 | 1016 | 1094 | 1746 | –15 |
| MP2/6-311++G(2df,2pd)[c] | 611 | 851 | 950 | 1091 | 1056 | 1121 | 1719 | 2 |
| B3LYP/TZP[b] | 569 | 837 | 866 | 1008 | 971 | 1040 | 1722 | –53 |
| B3LYP/6-311++G(2df,2pd)[c] | 601 | 831 | 915 | 1055 | 1023 | 1083 | 1736 | –20 |
| GGA-PBE/6-311++G(2df,2pd)[c] | 571 | 817 | 872 | 1014 | 980 | 1045 | 1689 | –57 |
| GGA-PBE/DZDP+f[d] | 573 | 824 | 875 | 1017 | 973 | 1050 | 1683 | –56 |
| GGA-PBE/DZDP+f (partial hess.)[d] | 576 | – | 875 | 1021 | 976 | 1055 | – | –57 |
| GGA-RPBE/DZDP+f (partial hess.)[d] | 570 | – | 861 | 1000 | 959 | 1031 | – | –74 |

a Experimental results from Ref. S3.

b. Theoretical results from Ref. 87.

c Theoretical results by Gaussian 03 (Ref. 70).

d. Theoretical results by our program.

**Table S4** Frequencies of a sulfate on a $Pt_3$ cluster in vacuum. The structure of the sulfate on the $Pt_3$ cluster is similar to the one shown in Fig. 5 (C). Partial hess. means that the frequencies were obtained by using the partial Hessian matrices of $SO_4$. The unit is $cm^{-1}$.

| | $\nu_1$ | $\nu_2$ | $\nu_3$ | $\nu_4$ | $\nu_5$ | $\nu_6$ | $\nu_7$ |
|---|---|---|---|---|---|---|---|
| MP2/6-311++G(2df,2pd)[a] | 613 | 614 | 628 | 918 | 977 | 979 | 1361 |
| B3LYP/6-311++G(2df,2pd)[a] | 574 | 574 | 600 | 870 | 886 | 887 | 1303 |
| GGA-PBE/6-311++G(2df,2pd)[a] | 534 | 535 | 557 | 807 | 846 | 848 | 1240 |
| GGA-PBE/DZDP+f[b] | 541 | 542 | 570 | 797 | 834 | 837 | 1238 |
| GGA-PBE/DZDP+f (partial hess.)[b] | 539 | 540 | 569 | 797 | 834 | 836 | 1238 |
| GGA-RPBE/DZDP+f (partial hess.)[b] | 534 | 535 | 563 | 785 | 821 | 824 | 1219 |

a Theoretical results by Gaussian 03 (Ref. 70).

b. Theoretical results by our program.

**Table S5** Frequencies of a bisulfate on a $Pt_2$ cluster in vacuum. Partial hess. means that the frequencies were obtained by using the partial Hessian matrices of $HSO_4$. The unit is $cm^{-1}$.

| | $\nu_1$ | $\nu_2$ | $\nu_3$ | $\nu_4$ | $\nu_5$ | $\nu_6$ | $\nu_7$ |
|---|---|---|---|---|---|---|---|
| MP2/6-311++G(2df,2pd)[a] | 592 | 594 | 813 | 1027 | 1101 | 1179 | 1371 |
| B3LYP/6-311++G(2df,2pd)[a] | 563 | 574 | 796 | 985 | 1034 | 1160 | 1323 |
| GGA-PBE/6-311++G(2df,2pd)[a] | 532 | 535 | 752 | 922 | 981 | 1127 | 1272 |
| GGA-PBE/DZDP+f[b] | 536 | 543 | 748 | 909 | 967 | 1119 | 1273 |
| GGA-PBE/DZDP+f (partial hess.)[b] | 535 | 542 | 748 | 910 | 967 | 1119 | 1273 |
| GGA-RPBE/DZDP+f (partial hess.)[b] | 529 | 537 | 730 | 899 | 956 | 1122 | 1255 |

a Theoretical results by Gaussian 03 (Ref. 70).

b. Theoretical results by our program.

**Table S6** Frequencies of a sulfate on a $Pt_3$ cluster and Pt(111) slab. Both results were obtained by using the GGA-PBE functional, DZDP+f basis set and the partial Hessian matrices of $SO_4$. The unit is $cm^{-1}$.

| | $\nu_1$ | $\nu_2$ | $\nu_3$ | $\nu_4$ | $\nu_5$ | $\nu_6$ | $\nu_7$ |
|---|---|---|---|---|---|---|---|
| Sulfate on $Pt_3$ cluster | 539 | 540 | 569 | 797 | 834 | 836 | 1238 |
| Sulfate on Pt(111) slab | 553 | 554 | 569 | 805 | 823 | 826 | 1238 |

**Table S7** Frequencies of a bisulfate on a $Pt_2$ cluster and Pt(111) slab. Both results were obtained by using the GGA-PBE functional, DZDP+f basis set and the partial Hessian matrices of $HSO_4$. The unit is $cm^{-1}$.

| | $\nu_1$ | $\nu_2$ | $\nu_3$ | $\nu_4$ | $\nu_5$ | $\nu_6$ | $\nu_7$ |
|---|---|---|---|---|---|---|---|
| Bisulfate on $Pt_2$ cluster | 535 | 542 | 748 | 910 | 967 | 1119 | 1273 |
| Bisulfate on Pt(111) slab | 533 | 560 | 752 | 923 | 936 | 1096 | 1260 |

## E. Displacement vectors of vibrational modes

The displacement vectors of vibrational modes for sulfate, bisulfate and hydronium-sulfate ion pair are summarized in Figs. S1, S2 and S3, respectively. Vibration frequencies and the corresponding squares of dynamic dipole moments are also shown in these figures.

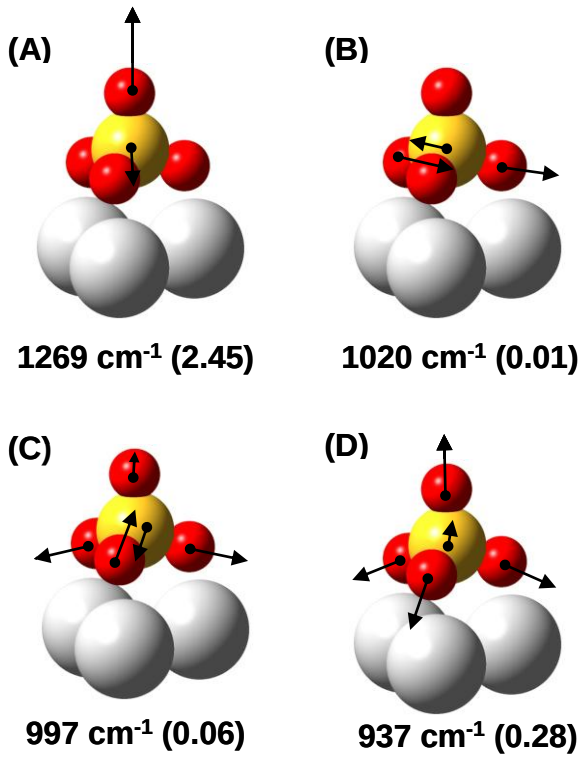


Figure S1 Displacement vectors of vibration modes for sulfate at 0.63 V (RHE). Values in the parenthesis are the squares of the dipole moments along the surface normal, the unit of which is $e^2$.

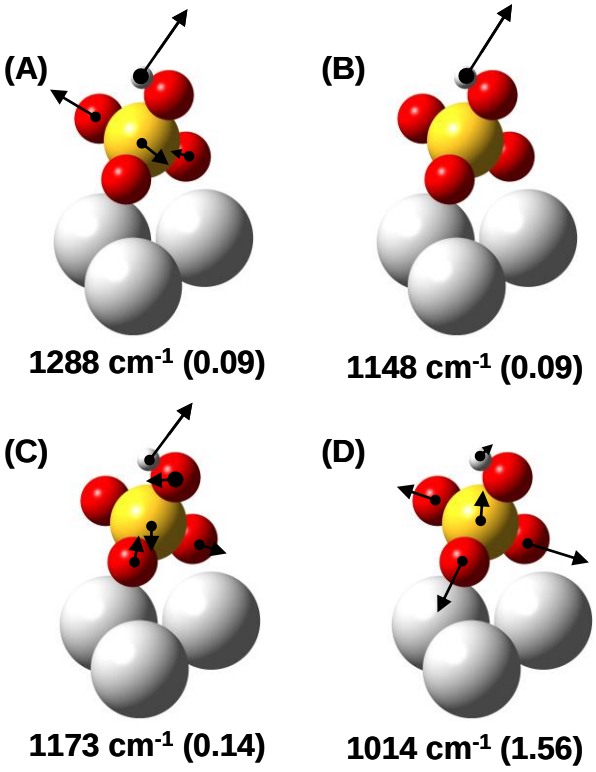


Figure S2 Displacement vectors of vibration modes for bisulfate at 0.50 V (RHE). Values in the parenthesis are the squares of the dipole moments along the surface normal, the unit of which is $e^2$.

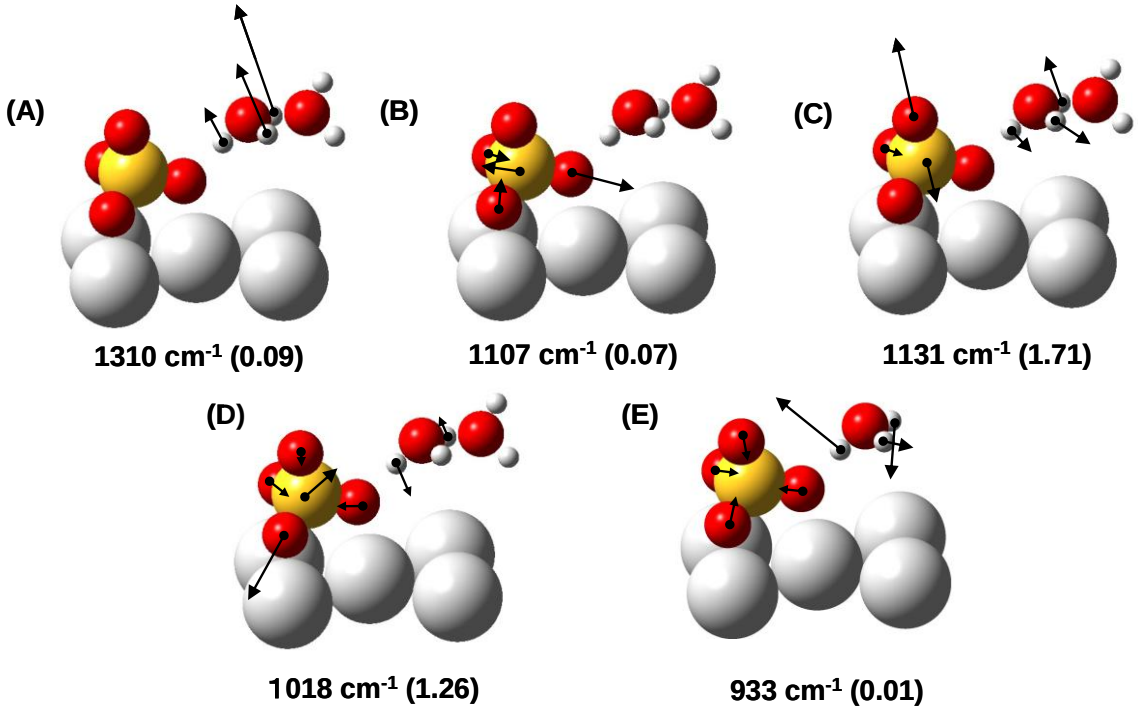


Figure S3 Displacement vectors of vibration modes for hydronium-sulfate ion pair at 0.46 V (RHE). Values in the parenthesis are the squares of the dipole moments along the surface normal, the unit of which is $e^2$.

## References

(S1) A. Givan, L. A. Larsen, A. Loewenschuss and C. J. Nielsen, *J. Chem. Soc. Faraday Trans.*, 1998, **94**, 827.

(S2) Y. –K. Choe, E. Tsuchida and T. Ikeshoji, *Int. J. Quantum Chem.*, 2009, **109**, 1984.

(S3) Y. Miller, G. M. Chaban, J. Zhou, K. R. Asmis, D. M. Neumark and R. B. Gerber, *J. Chem. Phys.*, 2007, **127**, 094305.